Journal of Neuroinflammation

RESEARCH

Open Access

Synergistic effects of repeated transcranial magnetic stimulation and mesenchymal stem cells transplantation on alleviating neuroinflammation and PANoptosis in cerebral ischemia

Shimei Cheng[1†], Qiying Lu[1†], Qiuli Liu[2†], Yuanchen Ma[4], Jinshuo Chen[1], Di Lu[2], Mudan Huang[1], Yinong Huang[3], Erming Zhao[2], Jing Luo[1] and Haiqing Zheng[1*]

Abstract

Background Neuronal death is the primary cause of poor outcomes in cerebral ischemia. The inflammatory infiltration in the early phase of ischemic stroke plays a vital role in triggering neuronal death. Either transplantation of mesenchymal stem cells (MSCs) derived from humans or repetitive transcranial magnetic stimulation (rTMS) have respectively proved to be neuroprotective and anti-inflammatory in cerebral ischemia. However, either treatment above has its limitations. Whether these two therapies have synergistic effects on improving neurological function and the underlying mechanisms remains unclear. This investigation aims to elucidate the synergistic effects and underlying mechanisms of MSCs combined with rTMS treatment on the neurological function recovery post-ischemia.

Methods A Sprague-Dawley rat model of cerebral infarction was induced via transient middle cerebral artery occlusion (tMCAO). The rats were divided into five groups ($n = 50$): sham, tMCAO, rTMS, MSCs, and MSCs + rTMS groups. Transplantation of human umbilical cord MSCs and rTMS intervention were performed 24 h post-stroke. Neurological function was further assessed via several behavioral tests and the 2,3,5-triphenyltetrazolium chloride (TTC) staining companied with Nissl staining were used to assess neuronal survival. TUNEL staining, western blotting, immunofluorescence, immunohistochemistry, ELISA, and flow cytometry were employed to measure the levels of neuroinflammation and PANoptosis. The molecular mechanisms underlying the special role of rTMS in the combined therapy were distinguished with transcriptome sequencing via PC12 cells in oxygen-glucose deprivation/reoxygenation (OGD/R) conditions.

[†]Shimei Cheng, Qiying Lu and Qiuli Liu contributed equally to this work.

*Correspondence:
Haiqing Zheng
zhenghq2@mail.sysu.edu.cn

Full list of author information is available at the end of the article

Results The combined therapy efficiently reduced lesion volume and improved neuronal survival ($P < 0.05$), subsequently improving functional recovery after ischemic stroke. MSCs + rTMS treatment ameliorated the PANoptosis in neurons ($P < 0.05$), accompanied by decreased levels of inflammatory factors in the cerebral tissue and serum during the subacute phase of cerebral infarction. To further explore the roles of either therapy on synergistic effect, we found that the transplanted MSCs primarily localized in the spleen and reduced cerebral inflammatory infiltration after ischemia via suppressed splenic inflammation. Meanwhile, rTMS significantly protects neurons from PANoptosis in MSCs-inhibited inflammatory conditions by downregulating REST unveiled by transcriptome sequencing.

Conclusions Our study elucidates an unidentified mechanism by which the combination of MSCs and rTMS could synergistically promote neuronal survival and suppress neuroinflammation during the subacute phase of cerebral infarction, thus improving neurological outcomes. The downregulating REST induced by rTMS may potentially contribute to the neuroprotective effect against PANoptosis in MSCs-inhibited inflammatory conditions. These results are expected to provide novel insights into the mechanisms of MSCs and rTMS combination therapy in synergistically protecting against cerebral ischemia injury and potential targets underlying neuronal PANoptosis in the early phase of stroke.

Keywords PANoptosis, Neuroinflammation, Programmed cell death, Combined modality therapies, Stroke

Introduction

Ischemic stroke is one of the most common diseases that causes disability and death worldwide [1]. It occurs when the brain blood flow is obstructed due to blockage of an artery, which leads to the deprivation of nutrients and oxygen to brain tissue and extensive neuronal death. While administering tissue plasminogen activator or endovascular thrombectomy can restore blood perfusion to preserve parts of neurons in the acute stage of cerebral infarction, the inflammation that follows in the subacute phase may cause significant damage to neural cells lasting up to ten days after the ischemic stroke [2–5]. It is the primary cause that contributes to worse neurological outcomes among survivors suffering from ischemia. However, even though neuroprotective intervention is urgently needed, it is crucial to develop effective strategies to mitigate inflammation response and rescue the neural cells in the subacute phase post-ischemic stroke to attenuate neurological disabilities.

Neuroinflammation plays an important role in secondary neuronal damage following ischemic stroke. The inflammatory response begins at the lesion site and then expands to surrounding tissue during the secondary phase. Meanwhile, a persistent inflammatory microenvironment after ischemic stroke is an important inducement of various programmed cell death (PCD) modes. Currently, mounting evidence demonstrates that various cell death occurs during ischemic stroke, including apoptosis, necroptosis, pyroptosis, necrosis, and PANnoptosis [6, 7]. PANnoptosis is a recently unveiled inflammatory PCD mode distinguished from other PCD modes, which could be induced by complex inflammatory cytokines and driven by caspases and RIPKs [8, 9]. Research demonstrated that PANoptosis is observed in ischemic brain injury in rat and mouse models [10]. Lan et al. demonstrated curcumin combined with olfactory mucosa-derived mesenchymal stem cells (OM-MSCs) inhibited neuronal PANoptosis by modulating microglial polarization [6], indicating that inhibition of neuroinflammation is a potential treatment for PANoptosis. However, how neuroinflammation is involved in PANoptosis and the mechanisms of alleviating PANoptosis in neurons in ischemic stroke remain to be explored.

In recent years, mesenchymal stem cells (MSCs) have attracted much attention for their ability to regulate inflammatory processes. It has been reported that multisource mesenchymal stem positively affected ischemic brain injury [11, 12]. Among the different types of stem cells, human umbilical cord mesenchymal stem cells (MSCs) have been preferred by researchers due to their accessibility, low immunogenicity, and few ethical controversies [12]. The therapeutic mechanisms of MSCs are multifaceted, but it is generally believed that these cells enable damaged tissues to form a balanced inflammatory and regenerative microenvironment under severe inflammatory conditions. Past research has shown that when exposed to an inflammatory environment, MSCs can coordinate local and systemic innate and adaptive immune responses by releasing a variety of mediators, including immunosuppressant molecules, growth factors, exosomes, chemokines, complement components, and various metabolites. Since the immunomodulatory capacity of mesenchymal stem cells is not constitutive and mediated by inflammatory cytokines, the outcome of mesenchymal stem cell activation may depend on the level and type of inflammation in resident tissues. Mounting evidence indicated that MSCs improved stroke outcomes potentially by inflammation modulation [13, 14]and improving neuron survival [15]. However, the efficiency of this therapy has been limited by the poor migration of MSCs to the ischemic lesions and low

implantation rate, which restricts their neuroprotective effect in turn.

Repetitive transcranial magnetic stimulation (rTMS) is one of the noninvasive brain stimulation techniques that is reported to be effective in improving outcomes in stroke patients [16–18]. It refers to the stimulation of the brain with a pulsed magnetic field. It was reported that Theta-burst rTMS promotes stroke recovery by vascular protection and neovascularization and reduces apoptosis of endothelial cells long-term at the late phase of stroke [19]. Sasso V et al. reported that rTMS significantly reduced neuronal death and glial activation in remote regions and improved functional recovery [20]. However, most of the studies focus on the effects of rTMS on the recovery phase, and little is known about the effects and mechanism of rTMS on the early phase of ischemic stroke. The underlying mechanism of how rTMS benefits neuronal survival is unclear.

Some studies have suggested that MSCs transplantation combined with rTMS may improve neural function recovery in central nervous system disease [21, 22]. However, the therapeutic effect of this combination therapy is still controversial, and the molecular mechanism underlying the synergistic effect needs further clarification. Whether MSCs transplantation combined with rTMS can ameliorate neuronal cell death in the early stage of ischemic stroke progression and the involvement of cell death way in ischemic stroke remains unclear.

Thus, in this study, using a rat model of transient middle cerebral artery occlusion (tMCAO) and neuronal oxygen-glucose deprivation (OGD) model, we aimed to explore the effect of MSCs transplantation combined with rTMS on neurological recovery in rats with cerebral infarction and determine whether MSCs transplantation combined with rTMS could orchestrate post-stroke neuronal inflammatory response and promote neuron function. We purposed to elucidate the potential mechanisms of this combined therapy to provide new treatment ideas and theoretical support for the treatment of ischemic stroke. In our study of neurological dysfunction resulting from cerebral infarction, we found that combination therapy indeed outperformed single treatments. Furthermore, we identified critical time points at which the combination therapy exhibited significant therapeutic advantages. Notably, we were the first to elucidate the specific mechanisms of action for the two treatments within the combination group, highlighting their superiority over the single treatment groups.

Materials and methods

Experimental animals

Male Sprague-Dawley (SD) rats (230–250 g, 6 ~ 8 weeks old) were purchased from Hunan SJA Laboratory Animal Co., Ltd (Changsha, PR China). The SD rats were raised in the specific pathogen-free (SPF) unit (three per cage) of the experimental animal center of South China Agricultural University, Guangzhou, China [license number: SYXK (Guangdong) 2022 − 0136]. All rats were housed under a 12-h:12-h light/dark cycle and 40-70% relative humidity in a temperature-controlled room (20–26 °C) with free access to food and water. All surgical procedures and animal care were conducted following the National Institutes of Health (NIH) Guidelines for the Care and Use of Laboratory Animals, also approved and reviewed by the South China Agricultural University Animal Ethics Committee (Approval no. 2022D148). A total of 250 rats were randomly assigned to five groups (n = 50 per group).

Cell culture

Human umbilical cord MSCs were provided by the Biotherapy Centre of the Third Affiliated Hospital of Sun Yat-sen University. Specifically, MSCs were successfully isolated and cultured in vitro from the umbilical cords of six healthy donors, who provided informed consent. The MSCs were cultured in a serum-free medium (Yocon, China) at 37 °C in a humidified incubator with 5% CO2 and 95% air. The medium was changed every 2 days commonly. When reaching 90% confluence, cells were detached by incubating with accutase (Thermo Fisher, A1110501, USA) for 5 min at 37 °C and then replated for continuous passage. MSCs within 6 cell passages were used for all experiments.

PC12 cell line (iCell) purchased from Guangzhou Taylor Biotechnology Co., LTD. Cells were cultured in 90% 1640 medium(GIBCO, USA) supplemented with 10% fetal bovine serum (FBS) (Procell, China), 100 IU/mL penicillin, and 100 μg/mL streptomycin (Thermo Fisher, USA) at 37 °C in a humidified incubator with 5% CO2 and 95% air. The medium was changed every 2 days. Following washed by phosphate-buffered saline (PBS)(GIBCO, USA) for 1 min, cells were detached by incubating with 0.25% trypsin (supplemented with EDTA) for 1 ~ 2 min at 37 °C when reaching 90% confluence and then replated for continuous passage.

Induction and treatment of tMCAO

The ischemic stroke model was induced by the right side of transient middle cerebral artery occlusion (tMCAO) as previously described [23, 24]. The tMCAO model is widely utilized in ischemic stroke research for high reproducibility and without craniotomy [25, 26]. Briefly, rats were anesthetized using 2% pentobarbital sodium (50 mg/kg, Sigma-Aldrich) via intraperitoneal injection. Afterward, the right common carotid artery (CCA), internal carotid artery (ICA), and external carotid artery (ECA) were exposed during the surgery. A filament (CINONTECH, China, A4-263650) was inserted

into the ICA to block blood flow from the origin of the middle cerebral artery. The duration of cerebral ischemia was 60 min. We have made all efforts to minimize animal suffering, including oral ibuprofen (60 mg/kg) (Macklin, China, I821809-25 g) to manage post-surgery pain and 1 h of constant temperature management (37 ℃) using a heating pad (20×35 cm; G-CLONE, China, VG-JRD-S) during anesthesia [27, 28]. After evaluation with modified neurological severity score (mNSS) [29], rats in the sham group with scores of 0 and tMCAO rats with moderate impairment (7 ~ 12 scores) were selected for this study, indicating the success of tMCAO establishment. Rats with mild impairment (1 ~ 6 scores) or severe impairment (13 ~ 18 scores) were excluded from the study. The mortality rate of tMCAO was less than 5% 24 h post-surgery, according to our experience, which is consistent with previous studies [26, 30].

For the treatment regimen, experimental rats were randomly assigned to 5 groups: Control group (tMCAO): 500 μL PBS(GIBCO, USA) was injected into the caudal vein; Repeated transcranial magnetic stimulation group (rTMS): 500 μL PBS was injected via a caudal vein and intervened with rTMS 1 d after tMCAO one time per day for 14 consecutive days; MSCs transplantation group (MSCs): 2×10^6 MSCs (per rat) were injected; Combination group (MSCs+rTMS): rats were injected with 2×10^6 MSCs (per rat) and treated with rTMS 4 h following MSCs transplantation one time per day for consecutive 14 d; sham group (sham): no 4−0 nylon suture was inserted, and the same volume of PBS was injected into the caudal vein as in the tMCAO group.

Differentiation, identification, and administration of MSCs

Osteogenic and lipogenic differentiation were conducted in vitro to assess the multidirectional differentiation potential. Briefly, human umbilical cord MSCs were seeded in a low glucose-DMEM (L-DMEM) (GIBCO, USA) complete medium prior to differentiation induction. Once the cells reached 80 ~ 90% confluence, the medium was replaced with bone induction medium containing L-DMEM, 10% FBS, 2 mM glutamine (GIBCO, USA), 100 IU/mL penicillin, 100 mg/mL streptomycin, 0.1 μM dexamethasone (Merck, USA), 50 μg/mL ascorbic acid (Sigma-Aldrich, USA) and 10 mM β-glycerol phosphate (Sigma-Aldrich, USA). After 2 ~ 3 weeks, osteogenic differentiation was confirmed by the mineralization of extracellular matrix and calcium deposits assessed using 0.5% Alizarin Red S (Sigma-Aldrich, USA) staining. Adipogenic differentiation was induced using adipogenic induction medium containing high glucose (H-DMEM) (GIBCO, USA), 10% FBS, 2 mM glutamine, 100 IU/mL penicillin, 100 mg/mL streptomycin, 1 μM dexamethasone, 10 μg/mL insulin (Prospect, Israel), 0.5 mM isobutylmethylxanthine (IBMX) (Sigma-Aldrich, USA) and 0.2 mM indomethacin (Sigma-Aldrich, USA) once the cells reached 100% confluence. Adipogenic differentiation was verified by the typical production of lipid droplet staining with Oil Red O (Sigma-Aldrich, USA).

The third passage human umbilical cord MSCs cultured in serum-free medium were digested with accutase at 37 ℃, resuspended to a concentration of 1×10^6/mL cell suspension, filtered through 70 μm sieve, and transferred to flow tubes, centrifuged for 5 min at 4 ℃, 450 × g, and resuspended in 100 μL PBS. Flow cytometric analysis was performed on LSR II (BD, USA) or CytoFLEX flow cytometer (Beckman Coulter, Fullerton, CA, USA), and data were analyzed using FlowJo7.6 software (Treestar, Ashland, USA). The utilized antibodies are listed in Supplementary Tables 1, and the corresponding isotype control antibodies were purchased from BD Bioscience. These antibodies were employed to label human umbilical cord MSCs at room temperature for the detection of cell phenotype via flow assay.

Human umbilical cord MSCs with sixth passage were digested with 0.25% trypsin (GIBCO, USA) at 37 ℃, and resuspended in PBS with a density of 4×10^6/mL MSCs. And 500 μL cell suspension (2×10^6/mL MSCs) was administrated per rat via a caudal vein 24 h after tMCAO surgery, according to previous studies [31, 32]. In brief, the rats were secured in a restrainer (Xiangbo, China, XB-DSL) measuring 230 mm (height) × 70 mm (outer diameter) × 60 mm (inner diameter), with the caudal vein exposed. The tail was wiped with alcohol for disinfection and to enhance the visibility of the caudal vein. An insulin syringe (BD, U-40, USA) was used to inject the MSC suspension into the caudal vein over a period of 10 to 15 s. After withdrawing the needle, pressure was applied to stop the bleeding, and the rats were released from the restrainer. Their vital signs were monitored for 30 min to ensure they were stable.

rTMS intervention

In vivo, a customized magnetic stimulator (CCY-IA, Wuhan Yiruide Medical Equipment, Wuhan, China) was used in this study to stimulate rats in the rTMS group and MSCs+rTMS group. The treatment was administered from 24 h to 14 days after tMCAO operation. All procedures followed a protocol described in previous studies [33]. Briefly, each rat was placed into a breathable rodent restraint bag (DecapiCones, Brain three Scientific, Braintree, MA, USA). A round prototype coil (6 cm in diameter with 3.5-T peak magnetic welds) was positioned perpendicular to the cortex on the surface of the cortical projection area of the ipsilateral primary motor cortex (right M1 zone) of each rat. The stimulation area of this coil covered a 1 ~ 2 cm^2 area of the brain, covering the peri-infarct region [34]. The rTMS group was applied at 10 Hz, with 40 pulses per train, 10 s intertrain interval,

and a total of 30 trains (1,200 pulses) for 7 min. The stimulation intensity was set to 26% of the maximum output strength of the machine, which is equivalent to 100% of the resting motor threshold (RMT). Motor-evoked potentials (MEPs) were measured at the right hind limbs and quadriceps femoris muscle using electromyography (MedelecSynergy; Oxford Instruments, Surrey, United Kingdom), as previously described [35]. The RMT was defined as the lowest stimulator output at which the peak-to-peak amplitude of the MEP was greater than 5% of its maximal amplitude in at least half of the 10 trials.

In vitro, followed by 24-hour reoxygenation, PC12 cells in 12-well plates were treated with rTMS every 8 h for 48 h. TMS treatment was conducted with a MagPro X100 magnetic stimulator (The MagVenture Company, Denmark) with a flat coin. The stimulation parameters were referred to a previous study [36]. Briefly, PC12 cells in the rTMS group and MSCs+rTMS group were applied at 10 Hz, 30% maximum output intensity of the machine, with 20 pulses per train, 10 s intertrain interval, and a total of 60 trains (1,200 pulses) for 11 min 44 s.

Survival rate and behavioral tests

The survival rate was documented every 24 h from the tMCAO surgery day until 14 days. We used the Zea Longa test, the Bederson test, the mNSS test, the cylinder test, and the adhesive removal test to assess the neurological deficit of rats before tMCAO surgery (0 days), and at 1, 4, 7, and 14 days after tMCAO in a blinded fashion. The experimenter was blinded to the group allocation.

The zea longa test

The Zea Longa test is a widely used method for assessing neurological deficits in animal models of stroke [26]. Briefly, neurological findings are evaluated on a five-point scale at 4 days post-stroke: a score of 0 indicates no deficits, while a score of 1 represents a mild focal deficit characterized by an inability to fully extend the left forepaw. A score of 2 indicates a moderate deficit, with the animal circling to the left, and a score of 3 reflects a severe deficit, where the rat falls to the left. Rats receiving a score of 4 do not walk spontaneously and exhibit a decreased level of consciousness.

The bederson test

The Bederson score test [37] involves lifting the rats' tails to a height of 10 cm above the table surface at 4 days post-stroke. At this point, normal rats will have their forelimbs extended, while animals with neurological deficits may exhibit the following behaviors: a score of 0: no deficits; a score of 1: when the tail is lifted, the forelimb on the paralyzed side is retracted and flexed under the abdomen, while the normal side extends toward the surface; a score of 2: aside from the behavior of a score of 1, when lying prone on the surface, there is significantly less resistance to pushing objects toward the paralyzed side compared to the normal side; a score of 3: aside from the behaviors of a score of 1 and 2, the animal rotates toward the paralyzed side while walking.

The mNSS test

We evaluated the neurological deficits using mNSS as described previously [29]: a score of 1~6 indicated mild impairment; a score of 7 ~ 12 indicated moderate impairment; and a score of 13 ~ 18 indicated severe impairment. The mNSS comprised a motor, sensory, balance, and reflex test. In brief, the rats were placed on a customized balance beam (20 mm × 20 mm × 200 mm), fixed at a height of 10 cm above the table surface, allowing the animals to walk along the wooden beam. The performance of rats was observed and scored according to the table entries [24], with each rat assessed three times.

The cylinder test

To evaluate the motor functional recovery, a cylinder test was performed at 0, 1, 4, 7, and 14 days post-stroke [34]. In brief, the rats were acclimated in a customized transparent colorless acrylic cylinder measuring 400 mm (height) × 200 mm (outer diameter) × 190 mm (inner diameter) for 5 min. Their forelimb placements against the cylinder wall were then observed and recorded for a total of 20 trials for three independent times. The score was calculated as: (number of ipsilateral forelimb placements - number of contralateral forelimb placements) / (number of ipsilateral forelimb placements+number of contralateral forelimb placements+bilateral forelimb placements).

The adhesive removal test

To detect the sensorimotor function, an adhesive removal test was performed at 0, 1, 4, 7, and 14 days post-stroke [38]. The investigator was blinded to the experimental groups for the evaluation and the statistical analysis. In brief, the rats were allowed to acclimate in a clean, customized, transparent glass box (300 mm × 400 mm × 600 mm)for 2 min before testing. A piece of tape (30 mm × 40 mm) was then applied to the paw pad of the contralateral side of the rats. In a quiet environment, the rats were allowed to move freely, and the time taken to notice the tape and the time taken to remove it were observed and recorded three independent times.

Perfusion and tissue preparation

For tissue preparation, rats were anesthetized with 2% pentobarbital sodium via intraperitoneal injection. A thoracotomy was performed, and the animals were manually perfused with PBS through the left ventricle. The rats were then decapitated, and the ipsilateral side of the

brain and the spleen were extracted for western blotting and flow cytometry. For frozen sections, rats were perfused with 4% paraformaldehyde (PFA) (Solarbio, USA) following perfused with PBS, and then the whole brain or the spleen was immersed in 4% PFA and stored at 4℃, followed by subsequent frozen slices.

Quantification of infarct volume

According to previous methods, we used 2,3,5-triphenyltetrazolium chloride (TTC) (Solarbio, China) staining to detect the quantification of infarct volume [39]. The fresh brains were quickly removed, frozen at −20 °C, and sliced into 2 mm-thick sections. The slices were then stained with a 2% solution of TTC at 37 °C for 30 min in the dark. Each brain slice's infarction area was measured using Image J analysis software. The infarct volumes were expressed (with correction for the edema) as a percentage of total hemispheres. Briefly, the volumes of the ipsilateral and contralateral hemispheres were counted, while the relative lesion volume was computed as follows: lesion volume=(area of contralateral hemisphere−area of normal region in the ipsilateral hemisphere)/area of contralateral hemisphere×100%.

Nissl staining

To investigate the neuroprotective effects of rTMS and/or MSCs, Nissl staining was conducted to evaluate neuronal survival and death. The tissue was fixed in 4% paraformaldehyde (PFA) (Biosharp, China) at 4°C for 24 h. Sagittal brain Sect. (10 μm) were mounted on slides for Nissl staining [40]. Specifically, the frozen sections were removed from the −20°C refrigerator and allowed to reach room temperature. They were then fixed with a tissue fixative for 15 min and rinsed with a gentle stream of water. The tissue sections were immersed in a toluidine blue staining solution (Servicebio, China) for 2–5 min for Nissl staining. Subsequently, they were washed with water, slightly differentiated with 0.1% glacial acetic acid (Aladdin, USA, A433223-500 ml), and finally washed with running water to terminate the reaction. The degree of differentiation was monitored under the microscope. After rinsing with running water, the sections were dried in an oven. The sections were immersed in clean xylene(Macklin, China, X823000-100 ml) for 10 min to achieve transparency, and then sealed with neutral gum. Nissl-stained images were captured using 20× microscopy. In interpreting the results, Nissl bodies in neurons appear as dark blue particles, while the nucleus is light blue and the background is also light blue. In normal, undamaged neurons, the Nissl bodies were large and numerous, and the nucleoli were prominent. In damaged neurons, the number of Nissl bodies may decrease or even disappear, and the cell spacing may increase.

Western blotting

Following anesthetization and cardiac perfusion, brain tissue was promptly excised from the injured area. Peri-infarct region tissues of the brain or PC12 cells were collected and lysed in 1×RIPA lysis buffer(Solarbio, China, R0020), with pre-added protease inhibitor(1:100, Solarbio, China, P6730-1 ml) and phosphatase inhibitor(1:100, Solarbio, China, P1260-1 ml). After centrifugation at 13,000 × g for 15 min at 4 °C, we collected the supernatant as the protein lysate. Sonication lysis at 80% power for 1 min (15 s for cells), shaking the protein supernatant for 5 s and resting for 5 s. A Pierce™ BCA protein Assay kit (Thermo Fisher, 23225, USA) was utilized to quantify the protein concentration. Subsequently, protein samples were separated by SDS-PAGE (EpiZyme, China, PG113) and transferred to a 0.45 μm or 0.20 μm pore-sized polyvinylidenedifluoride (PVDF) membrane (Millipore, USA). The membranes were incubated in blocking buffer (Tris-buffered saline containing 5% skim milk powder, Biosharp, BS102-500 g, China) at room temperature for 1 h and then incubated with certain primary at 4 °C overnight. The following day, after being washed three times with Tris-buffered brine Tween20 (TBST) solution, the PVDF membranes were incubated with the corresponding secondary antibodies at room temperature for 60 min. The utilized primary and secondary antibodies are listed in Supplementary Table 2. Finally, an enhanced chemiluminescence kit (Biosharp, BL520B, China,) was employed to detect the immunoreactive bands. To calculate the conjugation yield, we used gel band quantification by Image J software.

Immunofluorescence (IF)

Sections of brain tissue were subjected to immunofluorescence staining as described below. We used immunofluorescent staining to investigate the localization and expression level of NeuN, GSDMD, Caspase-8, ASC, RIPK3, Iba1, CD68, CD45, CD169, and TNF-α. Briefly, brain slices were attached to the glass slides, and PC12 cells were seeded and cultured on a 15 mm round coverslip (#801007, NEST, China) in 12-well plates. Brain slices or coverslips of PC12 cells were washed with PBS for 10 min, followed by fixation for 10 min with 4% PFA. Subsequently, Brain slices or coverslips of PC12 cells were permeabilized in 0.1% Triton X-100 for 10 min, followed by incubation with 3% BSA buffer (Sigma-Aldrich, V900933-100G, USA) for 60 min at room temperature. Finally, brain slices or coverslips of PC12 cells were incubated with corresponding primary and secondary antibodies in the dark (listed in Supplementary Table 2). Nuclei visualization was subjected to DAPI (#D9542, Sigma) staining for 3 min at room temperature. Images were acquired under fluorescence microscopy or using a

Leica confocal microscope. The mean fluorescence intensity was calculated by image J.

Immunohistochemical (IHC) staining

Brain slices of each group were fixed using transcardial perfusion and immersion in 4% PFA for 20 min. Brain slices were washed with PBS three times (5 min per time), following drying at 56 °C for 20 min. Following antigen repair with EDTA(ZS, ZLI-9067, China), brain slices were washed with PBS three times (5 min per time). The standard streptavidin-biotin-peroxidase complex was used in IHC staining. H_2O_2 (0.3%) solution was used to block endogenous peroxidase activity. The brain slides were incubated with primary antibodies overnight at 4 °C. After washing with PBS three times, the brain sections were incubated with horseradish peroxidase-conjugated secondary antibodies(Servisbio, GB23302, China) for 30 min at room temperature. The utilized primary antibodies are listed in Supplementary Table 2. A kit (Dako REAL™ EnVision™ Detection System, Peroxidase/DAB+, Rabbit/Mouse, #K5007) was used to amplify the staining. Subsequently, brain slices were counterstained with hematoxylin, dehydrated, and visualized by a bright field microscope (E100, Nikon, Japan). The percentage number of Ly6G-positive was determined in high-power fields (200×) of each brain slice. Images were analyzed using ImageJ.

TUNEL assay

After immunofluorescence staining of NeuN according to the procedure mentioned above, we used a TUNEL staining kit (Beyotime, C1088, China) to continue co-staining with NeuN to detect the apoptosis of neurons according to the instructions of the kit. In brief, after staining with the NeuN primary antibody and the corresponding secondary antibody, 100 μL of TUNEL equilibration buffer was first added to each slice and incubated for 5 min. Second, the equilibration buffer was discarded. Then, 50 μL of TUNEL reaction mixture containing 1 μL of TdT enzyme was added to each slice. Third, the slices were placed flat in a humid chamber and incubated in the dark at 37 °C for 2 h. Fourth, the reaction mixture was removed, and the slices were rinsed twice in a 1× PBS staining bath, each for 5 min. Next, the slices were washed three times with a buffer containing 0.1% Triton X-100 prepared in PBS, which contained 5 mg/mL BSA, each wash lasting 5 min to reduce background staining. Fifth, 2 μg/mL DAPI staining solution was added dropwise to each slice and incubated in the dark at room temperature for 10 min. After staining, the DAPI solution was gently removed, and the samples were rinsed three times in 1× PBS, each for 5 min. Finally, the samples were observed and analyzed using a Leica confocal microscope.

Enzyme-linked immunosorbent assay (ELISA) of cytokines in CSF and serum

Rats were anesthetized by intraperitoneal injection of 2% pentobarbital sodium (50 mg/kg). After reperfusion with pre-cooled saline flush, the abdominal cavity was opened layer by layer to isolate and expose the abdominal aorta. An appropriate amount of blood was withdrawn with a 10 mL syringe. The blood was naturally coagulated at room temperature for 10 ~ 20 min, centrifuged for 10 min (2000 rpm), and the supernatant was collected. Cerebrospinal fluid was obtained according to previous work [24]. IL-1β (YJ730206, MIbio, China), IL-6 (YJ730219, MIbio, China), and TNF-α (SU-b31063, MIbio, China) ELISA kits were used to determine the OD values of each cytokine in the serum and cerebrospinal fluid (CSF) samples according to the instructions of each kit. The linear regression equation of the standard curve was used to calculate the sample concentration.

Isolation and analysis of CFSE+ MSCs in the brain

To track the MSCs in the brain following transplantation via caudal veil, suspension of MSCs was reacted with 5,6- carboxyfluorescein diacetate, succinimidyl ester, hereafter referred to collectively as CFSE(ThermoFisher, C34570, USA). Briefly, sixth passage human umbilical cord mesenchymal stem cells (MSCs) cultured in serum-free medium were digested with Accutase at 37 °C. The cells were then resuspended in 1 mL of PBS, to which 1 μL of CFSE was added. The mixture was allowed to react for 20 min at room temperature, with gentle agitation during the staining period. Subsequently, the cells were briefly washed with serum-free medium to remove any residual dye from the quenching solution, then centrifuged at 800 rpm for 5 min to obtain a cell pellet. The pellet was washed once with PBS (GIBCO, USA) and diluted to a concentration of 4×10^6/mL in PBS to prepare the suspension for caudal vein injection.

To analyze CFSE+MSCs in the brain, mononuclear cells were isolated from brain tissue. Total cells were extracted using Percoll's isolation method and subsequently analyzed by flow cytometry. Briefly, rats were anesthetized via intraperitoneal injection of 2% pentobarbital sodium (50 mg/kg) and then perfused through the left ventricle with pre-cooled 1 × HBSS (GIBCO, USA) until the liver appeared pale. The brain tissue was immediately removed and placed in pre-cooled RPMI 1640 medium, where surface impurities were eliminated. The tissue was thoroughly homogenized using a cell screen with a 70 μm aperture, and the resulting homogenate was centrifuged at 2,000 rpm for 10 min at 4 °C. Following the removal of the supernatant, the cells were resuspended in 7 mL of RPMI 1640 medium at room temperature. To create a 30% Percoll separation solution, 3 mL of 100% Percoll was added and mixed with the cell suspension.

Next, 3 mL of 70% Percoll separation solution was added to a new 15 mL centrifuge tube. The 30% Percoll solution was then carefully layered on top of the 70% Percoll solution using a straw. The mixture was centrifuged at 2,000 rpm (with acceleration set to 3 and deceleration set to 2) for 30 min at 22 °C. After centrifugation, a distinct white layer of cells was observed between the 30% and 70% Percoll solutions, representing the mononuclear cells. Approximately 2–3 mL of this white cell layer was carefully transferred to a new centrifuge tube. Then, 10 mL of 1 × HBSS (containing 2% fetal bovine serum) was added, and the mixture was centrifuged at 2,000 rpm for 10 min at 4 °C. The cells were washed three times with 1 × HBSS. The isolated mononuclear cells were then resuspended in 1 × HBSS for flow cytometry analysis to determine the proportion of CFSE+cells (FITC channel). Flow cytometry was performed using a BD LSR flow cytometer, and the data were subsequently analyzed using FlowJo software.

In vitro oxygen-glucose deprivation/reoxygenation (OGD/R) model establishment and treatment

To investigate the effects of rTMS or/and MSCs in vitro, we used an oxygen-glucose deprivation/reoxygenation (OGD/R) model and a transwell co-culture model. The OGD 4 h/R 24 h model mimicked the cerebral ischemia-reperfusion damage in vitro. Briefly, when PC12 in 12-well plates reached 60% confluence, the 90% 1640 medium(added 10% FBS, 100 IU/ml penicillin, and 100 μg/ml streptomycin) was replaced into a glucose-free 1640 medium(Servicebio, G4538, China)and incubated in a 1% hypoxic incubator (ThermoFisher Technologies, USA) for 4 h at 37 °C. After 4 h of oxygen-glucose deprivation, the glucose-free 1640 medium was replaced into 90% 1640 medium (GIBCO, USA) supplemented with 10% FBS, 100 IU/mL penicillin, and 100 μg/mL streptomycin at 37 °C in a humidified incubator with 5% CO2 and 95% air for 24 h. The OGD/R model was successfully established.

For the treatment regimen, cells were subjected to 5 groups: PC12 cells without any intervention (control); PC12 cells suffered from OGD 4 h/R 24 h(OGDR) once the cells reached 60%~70% confluence; PC12 cells suffered from OGDR followed by rTMS treatment for every 8 h (OGDR+rTMS); PC12 cells suffer from OGDR followed by co-cultured with MSCs for 48 h (OGDR+MSCs); PC12 cells suffer from OGDR followed by co-cultured with MSCs for 48 h and rTMS treatment for every 8 h (OGDR+MSCs+rTMS). The co-culture between PC12 cells and MSCs was conducted by a transwell co-culture system.

Transwell co-culture system

PC12 cells (1×10^5 cells per well) were seeded in 12-well plates in 90% 1640 medium supplemented with 10% FBS, 100 IU/ml penicillin, and 100 μg/ml streptomycin at 37 °C in a humidified incubator with 5% CO2 and 95% air, and subjected to OGD/R modeling or control treatment when cells reached 60% confluence. At the onset of reoxygenation, a 4 μm Transwell chamber (size:12-well, Coning, #3401, USA) was placed atop the well plates, and MSCs suspension in a serum-free medium (2×10^5 cells per well) were seeded in the upper chamber. We subsequently put the upper chamber upon the 12-well plates with OGD/R modeling or control-treated PC12 cells as the lower chamber. Following 24 h of incubation, the cell suspensions from the 12-well plates were collected for western blotting and flow cytometry.

Apoptosis detection by flow cytometry

Annexin V-PI kit (A211-01, Vazyme, China) was used to detect the apoptosis of PC12 cells. According to the kit's instructions, PC12 cells in each group were first detached from 12-well plates by incubating with 0.25% trypsin (without EDTA) for 1 ~ 2 min at 37 °C after treatment for 48 h. About 5×10^5 cells per well were collected, centrifuged at 1800 rpm for 5 min at 4 °C, and removed the liquid supernatant. Next, the cells were washed by precooling PBS twice at 1800 rpm for 5 min at 4 °C. Then, cells were suspended in 100 μL 1× Binding Buffer. Finally, we added 5 μL Annexin -FITC and 5 μL PI staining solution into the cell suspension, incubated them for 15 min in the dark at room temperature, and detected the samples by flow cytometry within 1 h. All flow cytometric analyses were conducted with Gallios (Beckman Coulter) flow cytometers, and the data were analysed using the Kaluza (Beckman Coulter) software packages.

Cell viability assay

Cell viability was measured using a Cell Counting Kit-8 (CCK-8) (Dojindo, Kumamoto, Japan). When the PC12 cells were adherently cultured, PC12 cells(10^4 cells per well) were seeded in 96-well plates and cultured in 90% 1640 medium supplemented with 10% FBS, 100 IU/ml penicillin, and 100 μg/ml streptomycin at 37 °C in a humidified incubator with 5% CO2 and 95% air. When PC12 cells reached 60% confluence, PC12 cells in the MSCs group and MSCs+rTMS group were cultured with the medium supernatant of MSCs for another 48 h. Then, the medium was replaced with fresh medium containing 10 μl CCK8 reagent. Then plates were incubated for 2 h at 37 °C. Relative cell numbers were calculated by measuring the absorbance of each well at 450 nm using a multifunctional microplate reader (Spark 10 M, Switzerland).

RNA sequencing and bioinformatics analysis

To compare the gene profiles of the PC12 neurons, RNA sequencing was carried out in triplicate. Using TRIzol reagent and following the manufacturer's instructions (Invitrogen, USA), total RNA was isolated from PC12 neurons in the OGDR group, OGDR+MSCs group, and the OGDR+MSCs+rTMS group. We measured the concentrations of the entire RNA sample using a NanoDrop ND-2000 instrument. Illumina NovaSeq 6000 platform (Annoroad Gene Technology, Co., Ltd, Beijing, China) was used for RNA sequencing. The original fastq files were then processed with fastp(version 0.2.0) for quality control in order to remove the low quality reads and adapter. After quality control, reads were mapped to rat genome reference (version Rattus_norvegicus.mRatBN7.2) using Hisat2 (version 2.1.0). The Htseq-count(version 0.11.2) were used to generate the gene count matrix. DESeq2(version 1.40.1) were used to perform differential gene analysis. A P value<0.05 and absolute log2FoldChange value above 1 was considered statistically significant. The online database genemania (https://genemania.org/) and of trrust (and https://www.grnpedia.org/trrust/) were used to analyze protein-prote in interaction (PPI) networks.

Statistical analysis

Statistical analysis and plotting were performed using GraphPad Prism 9.0 software. All data were presented as the mean±S.E.M. from at least three independent experiments. Result of infarction volume and nerve function scores were analyzed by Two-Way ANOVA, ELISA results were analyzed by One-Way ANOVA, and qPCR results were analyzed by T-test. $P<0.05$ was considered statistically significant.

Results

MSCs transplantation combined with rTMS had a synergistic positive effect on post-ischemia neurological function

MSCs were successfully isolated and cultured in vitro from healthy donors. These cells exhibited a spindle-shaped fibroblast-like morphology and demonstrated differentiation potential for lipogenic and osteogenic lineages (Figure S1A-C). MSCs were characterized at passage three by flow cytometry. Analysis revealed that the culture-expanded MSCs expressed positive surface markers CD29, CD44, CD73, CD90, CD105, and CD166, while lacking expression of CD34, CD45, and HLA-DR (Figure S1D). To investigate the effects of MSCs combined with rTMS on cerebral ischemia, MSCs (2×10^6 cells in PBS) were transplanted to each rat via caudal vein injection, 24 h after the successful establishment of the tMCAO model, following 10 Hz rTMS treatment one time per day for 14 consecutive days (Fig. 1A(a)).

We found that MSCs transplantation combining rTMS treatment increased the survival rate in the tMCAO rat model (Fig. 1B). The survival rate of the sham group was 100%, significantly higher than the tMCAO group ($P<0.0001$). The survival rate of the MSCs+rTMS group on day 14 post-surgery was the highest among all three treatment groups, about 1.8 times compared to that of the tMCAO group ($P=0.0329$). Both the two monotherapy groups showed higher survival rates than the tMCAO group but did not differ in mortality ($P>0.05$). In addition, body weight was recorded from the first day after surgery. Following tMCAO surgery, the tMCAO group and all treatment groups experienced a decrease in body weight from the first to the seventh day compared to the sham group. By day 14, body weight began to increase. Notably, the MSCs+rTMS group had a higher body weight compared to the tMCAO group ($P=0.016$) on the seventh day post-surgery. However, no significant differences were observed between the MSCs group and the rTMS group in comparison to the tMCAO group ($P>0.05$) (Fig. 1C).

To investigate the synergistic effects of rTMS and MSCs on neurofunction post cerebral ischemia, several behavioral tests were performed on the 0, 1-, 4-, 7-, and 14-days post-stroke (Fig. 1A(b)). The Zea Longa test and Bederson test were used to preliminary evaluate the neurological function deficits on the 4 days post-stroke. We found that the Zea Longa and Bederson scores were significantly higher in the tMCAO group compared to the sham group ($P<0.05$). Notably, the scores in the combination treatment group were lower than those in the tMCAO group ($P<0.05$). However, no significant differences were observed among the tMCAO group, the MSCs group, and the rTMS group ($P>0.05$) (Figure S2). In order to thoroughly assess the neurological function of animals, a more comprehensive test, the mNSS test was used to reflect the overall neurofunction after ischemic stroke, including motor, sense, and balance functions. Compared to the sham group, rats in the other groups that experienced surgery all exhibited neurological deficits in varying degrees ($P<0.05$). We observed that the mNSS was significantly improved in the MSCs group and the MSCs+rTMS group compared with the tMCAO group on the 7 and 14 days post-surgery ($P<0.05$). The rTMS group showed an improvement in neural function later on day 14 post-surgery ($P<0.05$) (Fig. 1D). The cylinder test is usually used to evaluate motor function after brain injury. Herein, we found a striking improvement in motor function in the MSCs+rTMS group compared to the tMCAO group from day 4 post-surgery until day 14 post-surgery ($P<0.05$). Interestingly, the MSCs+rTMS group even exhibited a better motor function compared with the two treatments alone on day 14 after surgery ($P<0.05$) (Fig. 1E). The adhesive removal test was

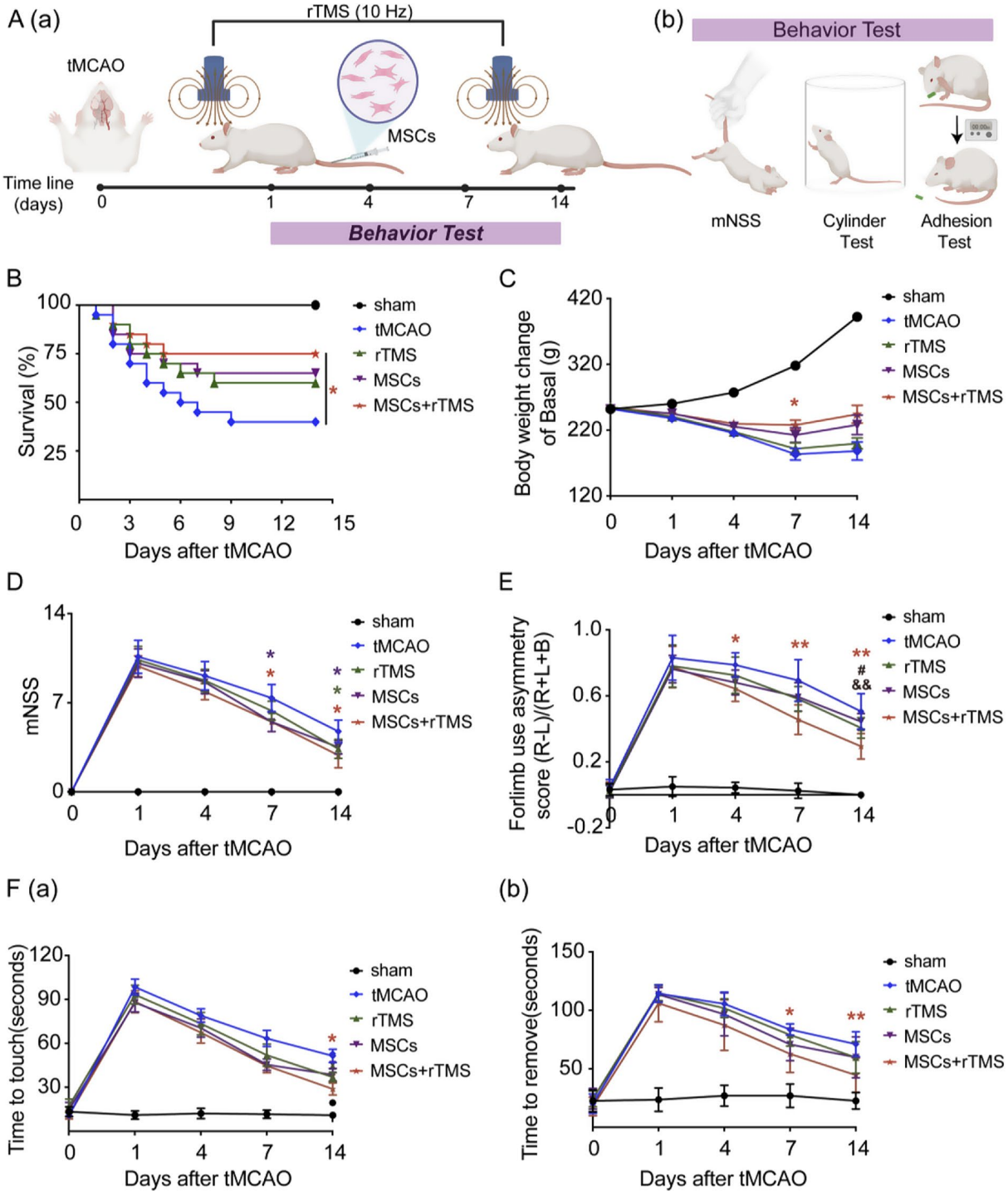

Fig. 1 Combining MSCs with rTMS treatment ameliorates neurological deficits in post-ischemic rats. (**A**)(a), Experimental design: MSCs transplantation was performed 24 h after the stroke. Behavioral tests were assessed at the indicated time points. rTMS was administrated following MSCs transplantation one time per day until animals were sacrificed. A(b), Schematic diagram of three behavioral tests. (**B**), The survival rates of each group were followed up every 24 hours for 14 days. n = 20 per group (**C**), The body weight of each group was tested at 0, 1, 4, 7, and 14 days post-stroke. n = 8 per group. (**D**), Neurological deficits were evaluated by the mNSS test for each group at 0, 1, 4, 7, and 14 days post-stroke. n = 8 per group. (**E**), Motor dysfunction was assessed by the cylinder test for each group at 0, 1, 4, 7, and 14 days post-stroke. n = 8 per group. (**F**), Sensorimotor dysfunction was assessed by the adhesive removal test up to 14 days post-surgery. Data were expressed as the latency to contact (**F**)(a) and remove (**F**)(b) tape from the contralateral forepaws. n = 8 per group. Asterisks, according to their color, indicate significant pairwise differences, *$P < 0.05$, ** $P < 0.01$ vs. tMCAO group; $^{\#}P < 0.05$ vs. rTMS group; $^{\&\&}P < 0$ 0.01 vs. MSCs group by two-way repeated-measures ANOVA and Tukey post hoc

performed to evaluate the sense function of rats. Only the combination treatment resulted in a significantly shorter time to touch and remove the tape compared to the tMCAO group ($P<0.05$) (Fig. 1F). The MSCs group and the rTMS group both showed an improvement in sense function compared with the tMCAO group, but there was no statistical significance ($P>0.05$). Taken together, the results above indicated that a combination of MSCs transplantation and rTMS therapy significantly improves post-stroke neurological recovery in vivo.

MSCs transplantation combined with rTMS promotes neuronal viability after cerebral ischemia

To assess infarct size, brain sections of each group were stained with 2,3,5-triphenyltetrazolium chloride (TTC). Following tMCAO surgery, infarct areas were observed in the tMCAO group and all treatment groups, while the sham group showed no infarct zones. We found a significant reduction in infarct volume in the MSCs+rTMS group compared to the tMCAO group on days 4 and 7 post-stroke ($P<0.05$). However, no significant differences were noted among the tMCAO group, the MSCs group, and the rTMS group ($P>0.05$) (Fig. 2A, B; Figure S3 A).

Microglia facilitate the infiltration of peripheral immune cells during the acute phase within 24 h post-ischemia [41–43]. However, our preliminary results indicate that combined treatment does not significantly affect microglial activation during the acute phase. Compared to the sham group, we observed a higher number of microglia in the tMCAO group and the three treatment groups. However, there were no significant differences among the four groups (Figure S3B, C). Neuronal destruction is a critical feature of ischemic stroke injury. To evaluate the extent of nerve damage across groups, we performed modified Nissl staining on days 1, 4, and 7 post-stroke, focusing on neuronal changes within the peri-infarct cortex (Fig. 2C, D). Ischemic damage typically leads to enlarged intercellular spaces, indicating cellular destruction. With Nissl staining, we observed a reduced number of viable neurons in the peri-infarct cortex of the tMCAO group compared to the sham group at all time points (all $P<0.001$). However, the degree of neuronal injury was mitigated by MSCs+rTMS treatment following tMCAO ($P<0.05$) (Fig. 2D-F). These findings suggested that the combination of MSCs and rTMS therapy effectively reduced neuronal damage and preserved a greater number of surviving neurons in the peri-infarct cortex during the subacute phase following stroke.

MSCs transplantation synergizes with rTMS to prevent PANoptosis in the subacute phase after ischemic stroke

To further investigate the mechanism of MSCs transplantation combined with rTMS in neuronal protection, we first examined various indicators of three typical PCD post-ischemia, apoptosis, pyroptosis, and necroptosis (Fig. 3A). Our results showed that the expression levels of apoptosis classical markers, caspase-3, and cleaved-caspase-3(c-caspase-3) increased in the tMCAO group compared to the sham group ($P=0.0218$; $P=0.0005$), while Bcl-2 level decreased($P=0.0197$). And the levels of Bax, caspase-3, and c-caspase-3 were significantly reduced by the combination treatment ($P=0.0021$; $P=0.0171$; $P=0.005$ versus tMCAO), whereas Bcl-2 expression was markedly increased ($P=0.0003$ versus tMCAO). This combination treatment demonstrated greater efficacy than rTMS alone in enhancing Bcl-2 expression ($P=0.0172$) (Fig. 3B(a)). Further immunostaining of TUNEL manifested that the number of apoptosis-positive neurons in the combination group was significantly lower than in the other groups within the ischemic penumbra region four days post-stroke ($P<0.0001$ versus tMCAO; $P=0.0031$ versus rTMS group; $P=0.00217$ versus rTMS group) (Figure S4). These findings indicated that MSCs transplantation combined with rTMS effectively prevented apoptosis during the subacute phase of ischemic stroke.

ASC, GSDMD, IL-18, IL-1β, NLRP3, and Caspaese-1 are recognized indicators of pyroptosis as reported a lot [44–47]. Our results showed that the expression levels of GSDMD, IL-18, IL-1β, NLRP3, and caspase-1 increased in the tMCAO group compared to the sham group ($P=0.0346$; $P=0.0002$; $P=0.0023$; $P=0.0006$; $P<0.0001$). The combination treatment significantly reversed the high expression levels of GSDMD, IL-18, IL-1β, NLRP3, and Caspaese-1 induced by ischemia($P=0.0055$; $P=0.0002$; $P=0.0109$; $P=0.01$; $P=0.0034$ versus tMCAO). Notably, the combination treatment also lowered the levels of IL-18 and IL-1β compared to rTMS treatment alone ($P=0.0417$; $P=0.0441$ versus rTMS group) (Fig. 3B(b)). Immunostaining manifested that GSDMD-positive neurons in the rTMS group, MSCs group, and MSCs+rTMS group were markedly decreased in the ischemic penumbra region four days after MCAO ($P=0.0119$; $P=0.0051$; $P<0.0001$; versus tMCAO), while no GSDMD-positive neurons were detected in the sham group. The reduction was further enhanced by the combination treatment, with significant differences observed when comparing the MSCs+rTMS group to the rTMS group ($P=0.0069$) and the MSCs group ($P=0.0159$) (Fig. 3C, D). These results manifested that MSCs transplantation combined with rTMS effectively lessened pyroptosis.

Necroptosis is one of the main modes of neuronal death in the subacute stage of ischemic stroke [48]. RIPK1, RIPK3, and MLKL are recognized indicators of necroptosis [47, 49]. Our results showed that the expression levels of total RIPK1(tRIPK1), phosphorylated (pRIPK1), and pMLKL were significantly elevated in the tMCAO group compared to the sham group ($P=0.0034$; $P<0.0001$;

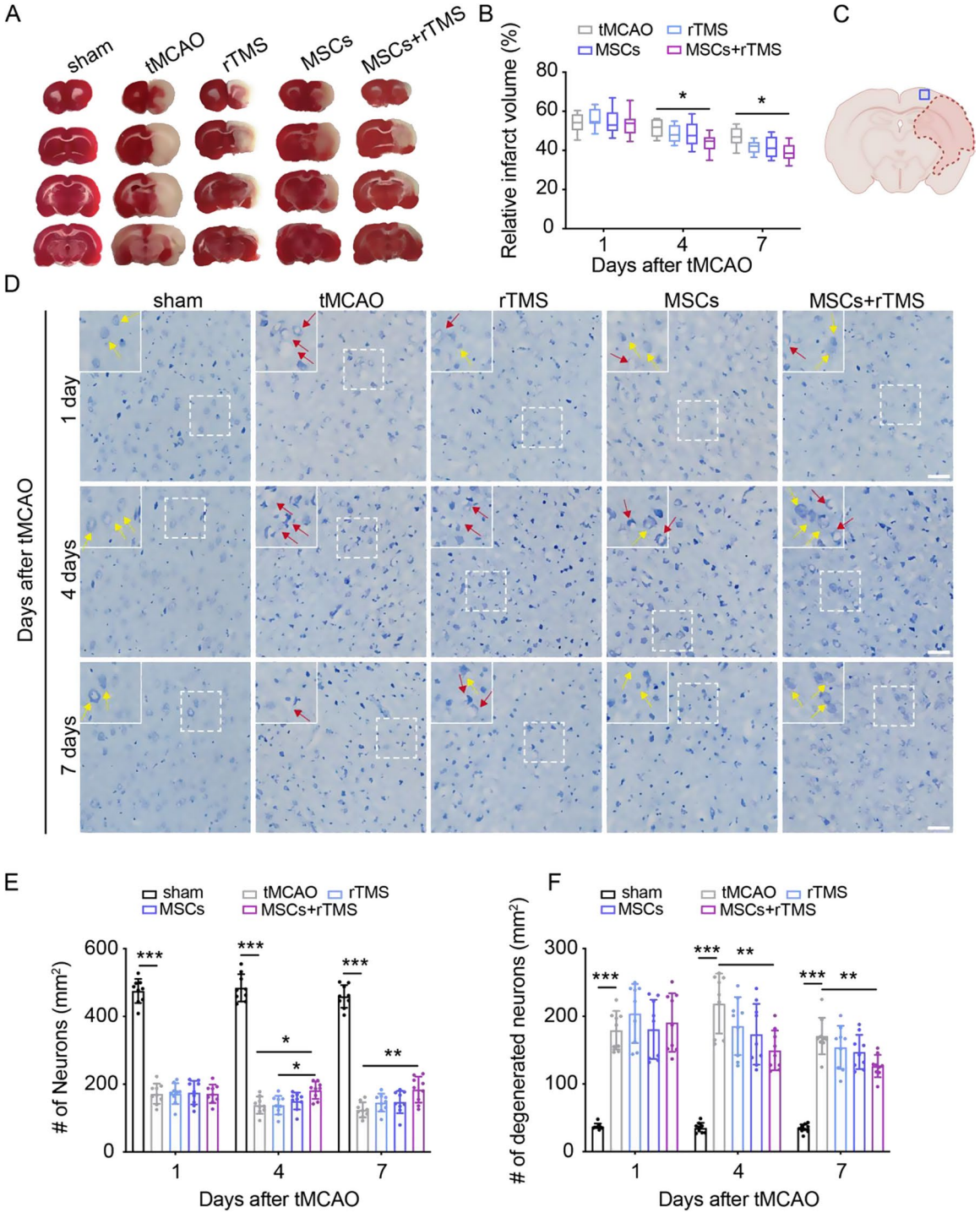

Fig. 2 MSCs combined with rTMS therapy reduce neuronal damage in the subacute phase after stroke. (**A**), Representative TTC staining images of the coronal brain sections of rats in the sham group, tMCAO group, rTMS group, MSCs group, and MSCs + rTMS group 4 days after tMCAO. (**B**), Bar graph showed quantification of infarct volume determined by TTC staining on day 1, day 4, and 7 after tMCAO surgery. n = 8 per group. (**C**), Diagram of the regions of the ischemic core and the peri-infarct region. (**D**), Neuronal degeneration in tMCAO rats with rTMS or/and MSCs therapy. Neurons (yellow arrows) and degenerating neurons (red arrows) were visualized using Nissl staining of brain sections in each group. The scale bar represents 50 μm. (**E**), Quantification of neurons was conducted in six randomized fields. n = 3 per group. (**F**), Quantification of degenerating neurons was conducted in three randomized fields. n = 3 per group. *$P < 0.05$, ** $P < 0\ 0.01$, *** $P < 0\ 0.001$ by one-way ANOVA and Tukey post hoc

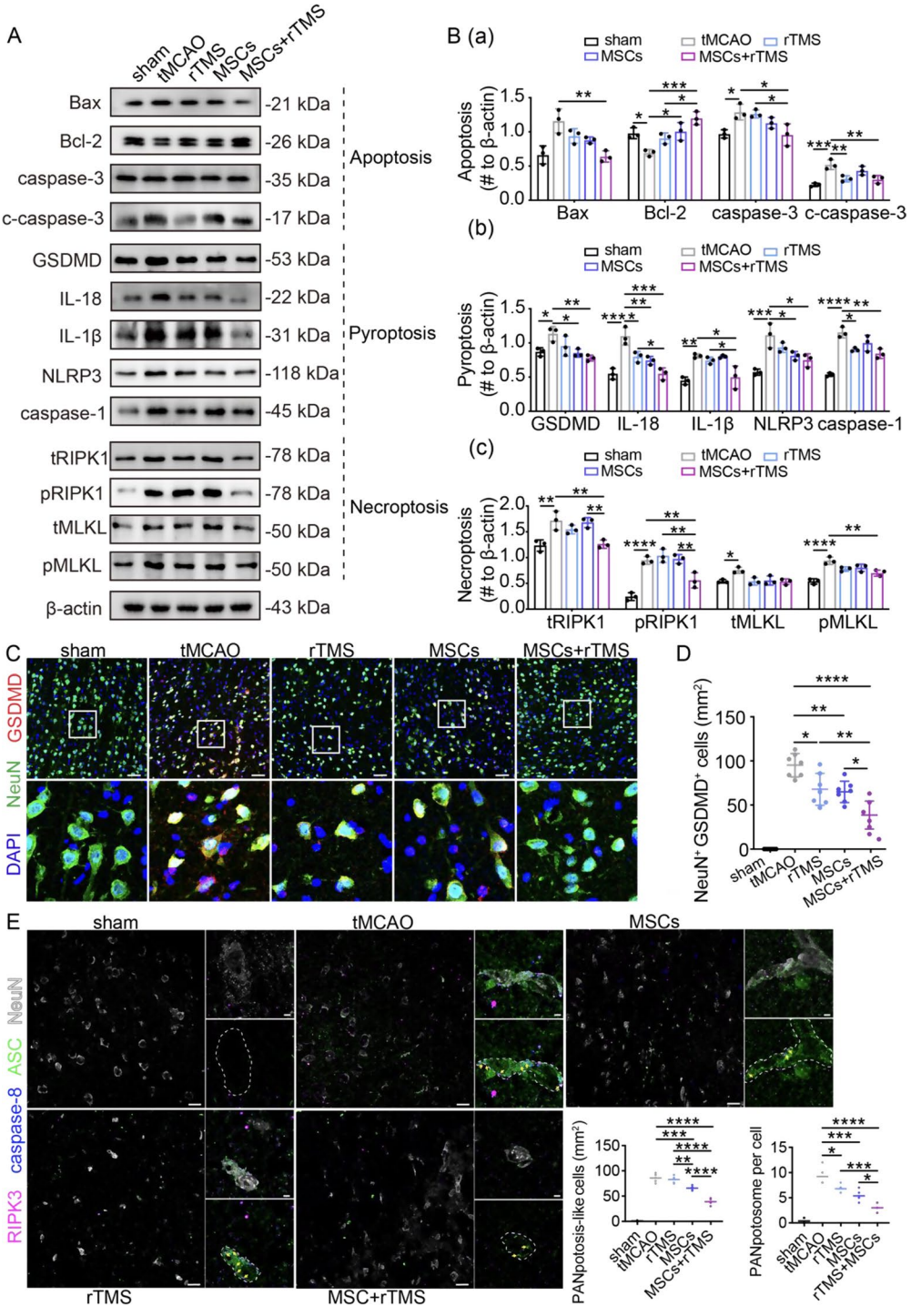

Fig. 3 Combining treatment rTMS with MSCs ameliorates PANoptosis during the subacute phase after stroke. (**A**), Representative immunoblot images of target protein in PANoptosis pathway 4 days after tMCAO in the peri-infarct cortex of rats. (**B**)(a), Quantitative analysis of protein level in apoptosis pathway 4 days after tMCAO in the peri-infarct cortex of rats. n = 3 per group. β-actin was used as the internal control. (**B**)(b), Quantitative analysis of protein level in pyroptosis pathway 4 days after tMCAO in the peri-infarct cortex of rats. n = 3 per group. β-actin was used as the internal control. (**B**)(c), Quantitative analysis of protein level in necroptosis pathway 4 days after tMCAO in the peri-infarct cortex of rats. n = 3 per group. β-actin was used as the internal control. (**C**), Fluorescent staining with DAPI (blue), NeuN (green), and GSDMD (red) showed pyroptosis of neurons 3 days after treatment. The scale bar represents 50 μm. (**D**), Quantitation of NeuN-positive and GSDMD-positive cells was conducted in seven independent scopes. (**E**), Fluorescent staining with RIPK3 (magenta), caspase-8 (blue), ASC (green), and NeuN (gray) showed PANoptosome in neurons 3 days after treatment. The spots(yellow arrows) represented PANoptosome. The quantitation of PANoptosis-like cells and PANoptosome was conducted in five independent scopes. The scale bar represents 20 μm in the left image and 3 μm in the magnification image. **P* < 0.05, ** *P* < 0 0.01, ****P* < 0.001, *****P* < 0.0001 by one-way ANOVA and Turkey post hoc

$P=0.0166$; $P<0.0001$). In contrast, the combination treatment group exhibited decreased levels of tRIPK1, pRIPK1, and pMLKL ($P=0.0051$; $P=0.0088$; $P=0.0045$ versus tMCAO). However, no significant differences were observed in the expression of tMLKL among all groups (all $P>0.05$) (Fig. 3B(c)). These findings suggested that MSCs transplantation combined with rTMS sufficiently curtailed necroptosis. Unedited full gels for all western blots were provided in Figure S6.

Considering all the data above, we identified that all three forms of PCD, collectively referred to as PANoptosis—a newly identified form of PCD mediated by caspase-8 [50]—occur in ischemic stroke. Additionally, MSC transplantation combined with rTMS was found to alleviate this process. For further identify the PANoptosis-like cells, we detected the colocation of ASC, caspase-8, and RIPK3 which are the main composition of PANoptosome, a multiple-protein structure that occurred in cells with PANoptosis [44, 45]. Interestingly, we did not observe any PANoptosome in the sham group, but there are a lot in the tMCAO group indeed. Additionally, compared with the tMCAO group, PANoptosis-like cells significantly reduced in the combination treatment group (Fig. 3E). The above results indicated that MSCs transplantation combined with rTMS treatment can alleviate PANoptosis in rats with ischemic stroke.

MSCs reduce the inflammatory infiltration in the central nervous system via inhibiting splenic immunity

Since the combination of MSC transplantation and rTMS treatment exhibited a synergetic effect on neural protection, we further proposed investigating the role of each of the two treatments. Inflammation after ischemic stroke is the primary cause of inflammatory cell death, such as pyroptosis, necroptosis, and recently emerged PANoptosis [6, 7]. As is known, MSCs show positive effects on repairing damaged tissues and organs mainly by secreting anti-inflammatory cytokines to reduce inflammation and apoptosis of tissue cells [51].

Herein, we investigated the inflammation of the brain after MSCs transplantation or rTMS treatment to determine the role of MSCs in the efficacy of combination therapy. Activation of microglia and astrocytes in the early phase post-stroke results in pro-inflammatory cytokines production, such as TNF-α, IL-1β, and IL-6, which circulate throughout the body and cause systemic inflammation [52]. The expression of IL-6 decreased in the tMCAO group compared to the sham group($P=0.0009$). We observed that only the combination therapy dramatically decreased the level of IL-1β and TNF-α ($P<0.05$) in the cortex, while the two monotherapy groups did not show any significant differences compared to the tMCAO group. However, all the three strategies of treatment could alleviate the expression of IL-6 ($P<0.05$) (Fig. 4A, B). Unedited full gels for all western blots were provided in Figure S6. A similar situation of the levels of IL-1β, IL-6, and TNF-α was also observed in the cerebrospinal fluid (CSF) of the MSCs+rTMS treatment group by ELISA compared to the tMCAO group ($P<0.05$). But different from the condition in the cortex, the levels of IL-6 and TNF-α in the CSF of the MSCs treatment group obviously declined in comparison to that in the tMCAO group ($P<0.05$) (Fig. 4C). It suggested that MSCs treatment may not only contribute to the central immunosuppression.

Next, we tended to explore the effect of combined therapy on the systemic inflammatory infiltration post-stroke. Ly6G is a primary marker for neutrophils, involved in acute inflammatory responses and promoting immune cell recruitment and bacterial clearance. In rodents, $Ly6C^+$ cells typically represent monocytes and certain types of T cells, participating in inflammatory responses and tissue repair. The phenotype of the $Ly6G^+/Ly6C^+$ cells labels neutrophils [53]. Compared with the sham group, the tMCAO group had a significant increase in $Ly6G^+/Ly6C^+$ cells($P<0.0001$). Moreover, $Ly6G^+/Ly6C^+$cells were significantly decreased in the MSCs group and MSCs+rTMS group, compared with the tMCAO group ($P<0.05$), while the rTMS group did not show a decrease compared with the tMCAO group (Fig. 4D). These findings suggested that the systemic inflammatory infiltration in the central nerve system was suppressed by MSCs transplantation. Macrophages are the periphery immune cells that migrate to the infarct area on the heels of neutrophils. Iba1 serves as a specific marker for microglia, the resident immune cells of the central nervous system. And CD68 is a specific marker for M1 macrophages, the proinflammatory macrophages that respond to the early immune response after stroke, indicating systemic inflammatory infiltration in the brain here [54]. Compared with the sham group, the number of $CD68^+$ cells significantly increased in the tMCAO group ($P<0.0001$). Compared with the tMCAO group, $CD68^+$ cells were strikingly decreased in the MSCs group and MSCs+rTMS group($P<0.05$). And there was no significant difference between the rTMS and tMCAO groups, and the number of $CD68^+$ cells in the rTMS group was even higher than that in the MSCs+rTMS group ($P<0.05$) (Fig. 4E). $CD68^+$ cells and $Iba1^+$ cells are rarely co-labeled, indicating that CD68 originates from macrophages in the blood circulation. We also observed that the TNF-α in serum was lower in the MSCs group or MSCs+rTMS group than in the tMCAO group ($P<0.05$) (Fig. 4F). It suggested that systemic transplantation of MSCs may alleviate inflammation response in both injured brain and blood circulation, and the underlying mechanism needs further investigation.

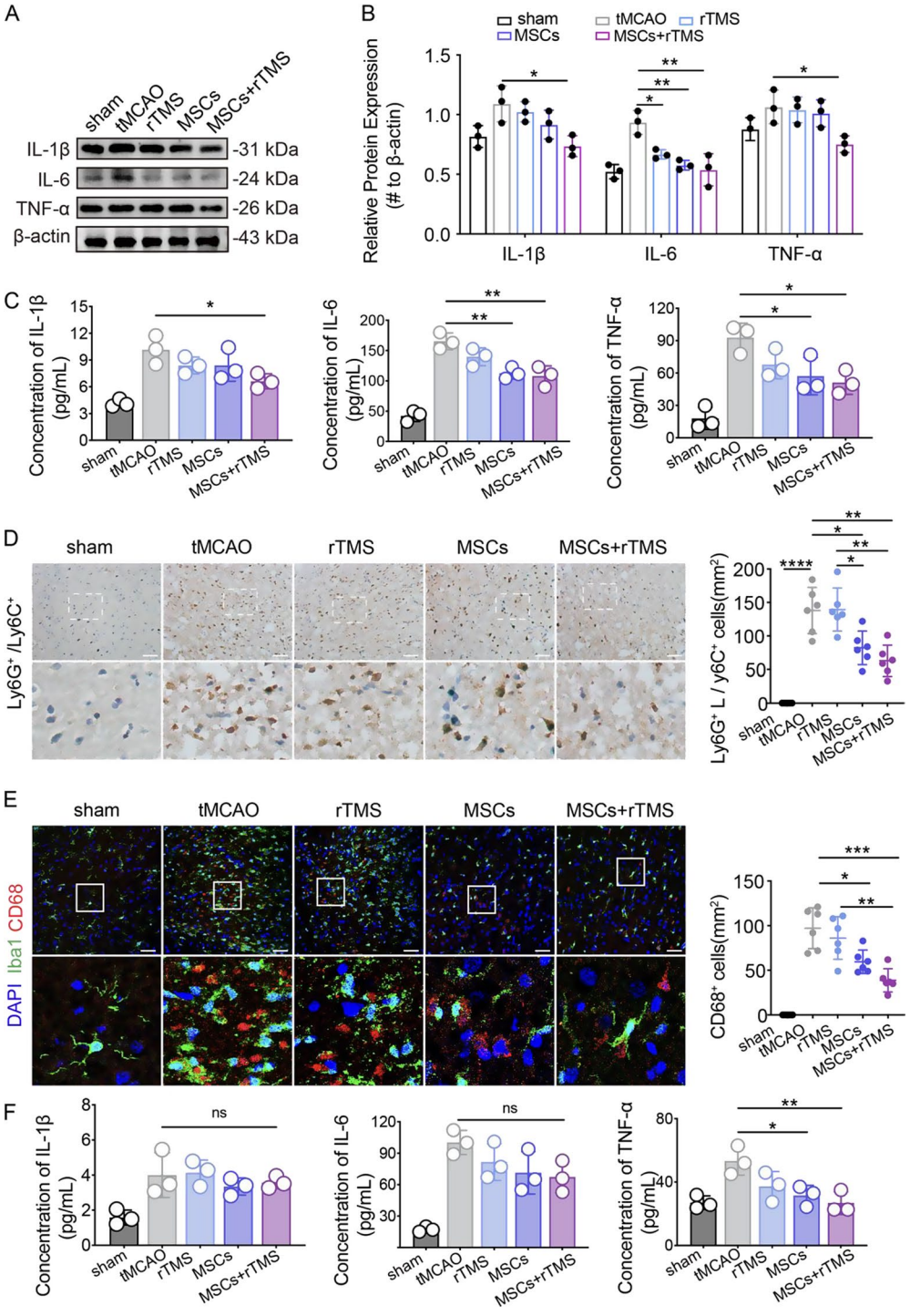

Fig. 4 .MSCs reduce the inflammatory infiltration in the central nervous system. (**A**), Representative immunoblot images of pro-inflammation factor 4 days after tMCAO in the peri-infarct cortex of rats. (**B**), Quantitative analysis of protein level of IL-1β, IL-6, TNF-α 4 days after tMCAO in the peri-infarct cortex of rats. n = 3 per group. β-actin was used as the internal control. (**C**), Concentration of IL-1β, IL-6, and TNF-α in CSF 3 days after treatment by ELISA. n = 3 per group. (**D**), Immunohistochemistry with Ly6G+/ Ly6C+, tawny spot showed neutrophils and monocytes, and the quantitation of them was showed by right, conducted in six independent scopes. n = 3 per group. Scale bar: 50 μm. (**E**), Fluorescent staining with DAPI (blue), Iba1 (green), and CD68 (red) showed periphery macrophage 3 days after treatment. The quantitation of them was shown by right, conducted in six independent scopes. n = 3 per group. Scale bar: 50 μm. (**F**), Concentration of IL-1β, IL-6, and TNF-α in serum 3 days after treatment by ELISA. n = 3 per group. **P* < 0.05, ** *P* < 0 0.01, ****P* < 0.001, *****P* < 0.0001 by one-way ANOVA and Turkey post hoc. ns refers to no significance.

In the past, it was believed that MSCs were involved in tissue regeneration through self-differentiation to replace the injured tissue, but now it is preferred that the efficacy of MSCs mainly attributed to the paracrine production of beneficial cytokines and inflammation modulation [51]. To figure out how MSCs exhibit efficacy and whether rTMS influences the planting of MSCs in the ischemic area, we traced the MSCs after injection into rats. But little MSCs were observed in the brain. And there were no significant differences among these three groups, the sham+MSCs group, the tMCAO+MSCs group, and the tMCAO+MSCs+rTMS group (Fig. 5A, B). Further quantitation by flow cytometry also showed that little MSCs can be found in the brain, with no more than 1% in the contralateral brain and no more than 4% in the ipsilateral brain (Fig. 5C, Figure S5A). Surprisingly, rTMS did not increase the engraftment of MSCs in the brain, whether in the contralateral or the ipsilateral brain. This implicated that the efficacy of combination therapy is not due to the increase of MSCs translocation into the injured region via rTMS. Thus, the MSCs-mediated immunosuppression post-ischemia may not mainly be attributed to the direct interaction in the infarct area. In view of the above findings, to further uncover the role of MSCs in combined therapy, we put our sight to the spleen, which is the source of peripherally infiltrating immune cells. The spleen is one of the most important major reservoirs of immune cells. During the acute phase, stroke induces the mobilization of more leukocytes from the spleen and triggers serials neurogenic pathways [55–57]. Interestingly, the spleen weight in the MSCs group and the MSCs+rTMS group was restored compared to that in the tMCAO group ($P=0.0195$, $P=0.0014$) (Fig. 5D, E). To characterize the various regions of the spleen, CD45, and CD169 were respectively used for delineating the red pulp and the marginal zone [58]. We found that a large number of the MSCs accumulated in the marginal zone (MZ) of the spleen, as reflected by the IF staining of CD169 (Fig. 5F). This was consistent with our previous work [57]. After ischemic stroke, compared to the sham group, the spleen weight in the tMCAO group significantly decreased ($P=0.0007$). Within a few minutes after stroke, damaged associated molecular patterns (DAMPs) actively secreted by dead or stressed cells or immune cells in the ischemic brain initiate a peripheral immune response, triggering acute systemic inflammation [58]. The expression level of TNF-α of the spleen in the MSCs group and the MSCs+rTMS group was also dramatically lower than that in the tMCAO group ($P<0.05$), whereas little TNF-α was observed in the sham group (Fig. 5G-J). Unedited full gels for western blots were provided in Figure S6. This suggested that MSCs decreased the immunization mobilization in the spleen.

rTMS ameliorates neural death in MSCs-inhibited inflammatory conditions via repressing REST

To further explore the contribution of rTMS on the combination efficacy in vitro. PC12 cells and MSCs were co-cultured in vitro by a transwell chamber system to simulate MSCs transplantation in vivo (Fig. 6A). And OGD/R model was established to mimic the glucose and oxygen deprivation of stroke. We observed that only the combination therapy significantly increased the cell viability of PC12 cells compared with the OGDR group ($P=0.0092$), while rTMS or MSCs monotherapy did not (Fig. 6B). Flow cytometry unveiled that rTMS did not significantly decrease the apoptosis rate. However, when rTMS was combined with MSCs, a reduction in apoptosis was observed (Fig. 6C, D).

The efficacy of combination treatment in vitro was consistent with those in vivo (Fig. 6E). In vitro, rTMS or MSCs alone did not significantly change the expression of Bax and Bcl-2 compared to the tMCAO ($P>0.05$). The combination of rTMS and MSCs strikingly decreased the expression of Bax and increased Bcl-2 in OGD/R-PC12 cells compared with the tMCAO group ($P<0.05$). Moreover, the combination group showed a decreased expression of Bax in the combination group compared to the OGDR+MSCs group or the OGDR+rTMS group. Compared with the control group, the expression of caspase-3 was significantly increased in the OGDR group ($P=0.0003$). The expression of caspase-3 in the combination group was significantly lower than that in the OGDR group or OGDR+MSCs group ($P<0.05$). MSCs monotreatment or MSCs+rTMS dramatically lowered the expression of c-caspase-3 ($P<0.05$), the active form of caspase-3 (Fig. 6F(a)). The combination treatment seems to have little effect on the pyroptosis of PC12 cells compared with the other two death ways, unlike in vivo. MSCs, rTMS, and combination treatment lowered the expression of IL-18, but the combination treatment group did not show a significant effect. Unfortunately, the expression of GSDMD, IL-1β, NLRP3, and caspase-1, important indicators of pyroptosis, did not differ among the OGDR group and treatment groups ($P>0.05$) (Fig. 6F(b)). tRIPK1 and tMLKL did not differ between OGDR and all treatment groups. The group of MSCs or rTMS alone did not change the expression of pRIPK1 compared to the OGDR group ($P>0.05$). However, the expression of pRIPK1 in the OGDR+MSCs+rTMS group was significantly lower than in the OGDR group and even the OGDR+rTMS group. Likewise, pMLKL in the OGDR+MSCs+rTMS group was lower than in the OGDR+MSCs group ($P<0.05$) (Fig. 6F(c)). These results manifested that rTMS ameliorates neural death in MSCs-inhibited inflammatory conditions.

To further reveal the potential regulatory mechanisms, RNA sequencing was conducted using

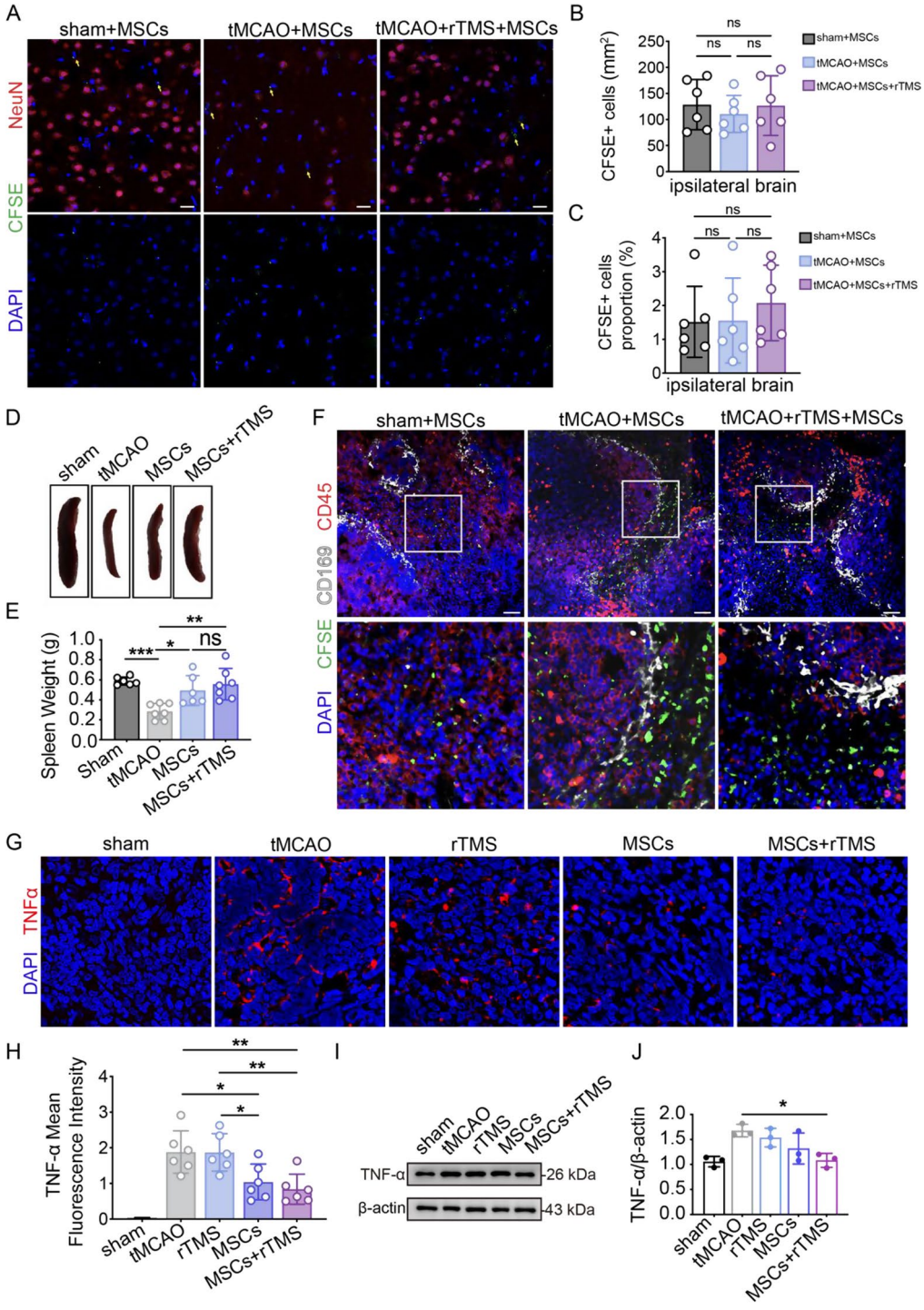

Fig. 5 MSCs inhibit splenic immunity. (**A**), Fluorescent staining with DAPI (blue) and NeuN (red), with tissue autofluorescence of CFSE (green) showed the number of exogenous MSCs that cross the blood-brain barrier into the brain parenchyma one day after injection. Yellow arrows to indicate the CFSE fluorescence of MSCs. n = 3 per group. Scale bar: 50 μm. (**B**), The quantitation of CFSE+ cells of the ipsilateral brain by fluorescent staining. n = 3 per group. (**C**), The quantitation of CFSE+ cells of the ipsilateral brain by flow cytometry. n = 3 per group. (**D**), The spleen was isolated from rats in each group. (**E**), The quantitation of the spleen weight in each group, n = 7 per group. (**F**), Fluorescent staining with DAPI (blue), CD45 (red), and CD169 (gray), with tissue autofluorescence of CFSE (green) showed the number of exogenous MSCs planted in the spleen 1 day after injection. n = 3 per group. Scale bar: 50 μm. (**G**), Fluorescent staining with DAPI (blue) and TNF-α (red) showed the expression of TNF-α in the spleen 3 days after MSCs injection. Scale bar: 50 μm. H, The quantitation of TNF-α expression in the spleen of each group. n = 6 per group. I, Representative immunoblot images of TNF-α 4 days after tMCAO in the spleen of rats. J, Quantitative analysis of protein level of TNF-α 4 days after tMCAO in the spleen of rats. n = 3 per group. β-actin was used as the internal control. *$P < 0.05$, ** $P < 0.01$, by one-way ANOVA and Turkey post hoc

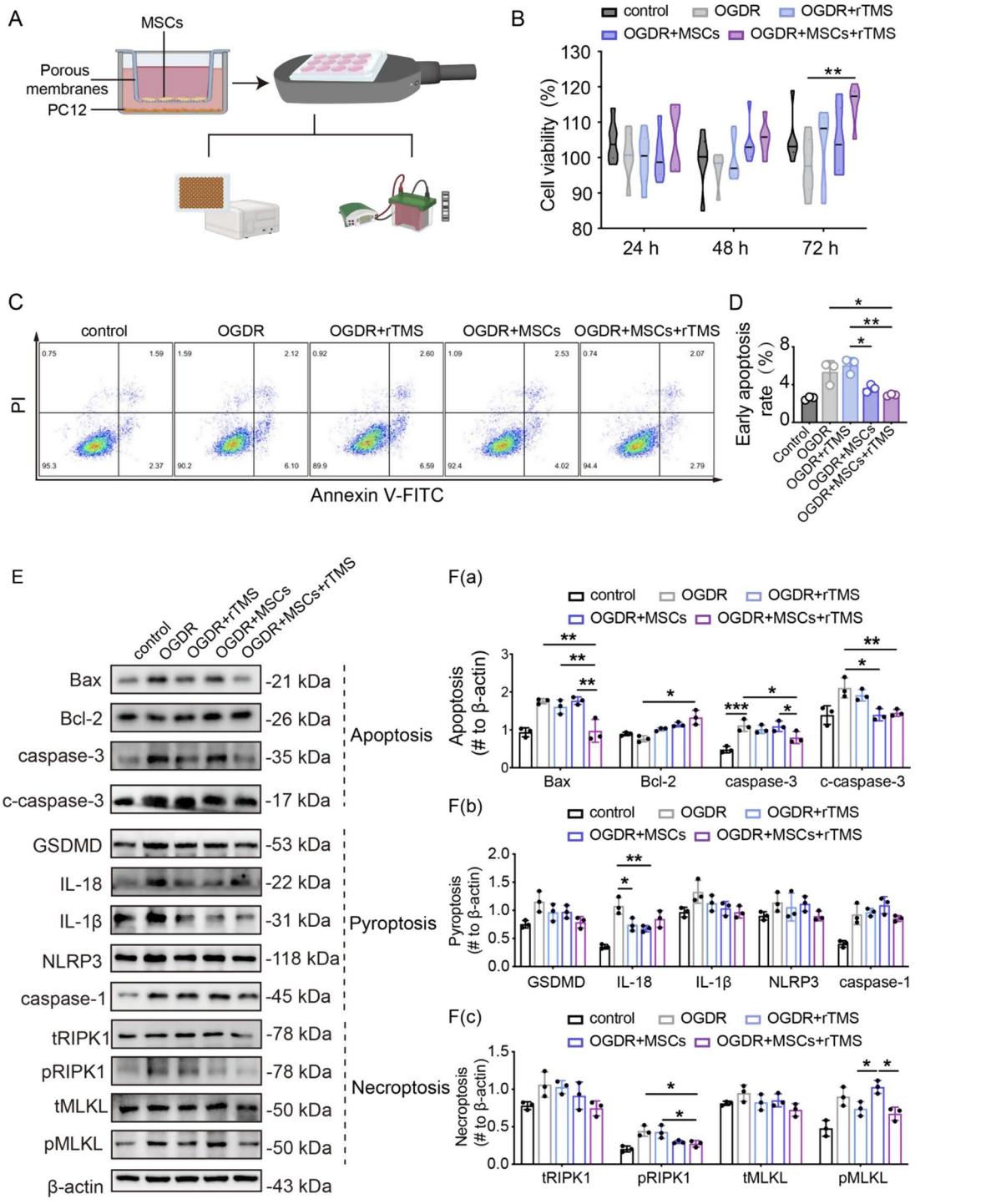

Fig. 6 rTMS ameliorates neural death in MSCs-inhibited inflammatory conditions. (**A**), Illustration of experimental design: After 24h of recovery following OGD 48h, PC12 cells were co-cultured with MSCs which were cultured in the 0.4 μm-pore transwell chamber beforehand. rTMS was performed immediately following OGD4h / R24h, every 8h, for a consecutive 48h. (**B**), Cell viability of PC12 cells was tested by CCK8 kit. n = 6 per group (**C**), Apoptosis of PC12 cells of each group by flow cytometry. (**D**), Quantitation of early apoptosis rate in each group. n = 3 per group. (**E**), Representative immunoblot images of target protein in PANoptosis pathway 2 days after OGD/R in PC12 cells. (**F**)(a), Quantitative analysis of protein level in apoptosis pathway 2 days after OGD/R in PC12 cells. n = 3 per group. β-actin was used as the internal control. (**F**)(b), Quantitative analysis of protein level in pyroptosis pathway 2 days after OGD/R in PC12 cells. n = 3 per group. β-actin was used as the internal control. (**F**)(c), Quantitative analysis of protein level in necroptosis pathway 2 days after OGD/R in PC12 cells. n = 3 per group. β-actin was used as the internal control. **P* < 0.05, ** *P* < 0.01, ** *P* < 0.001 by one-way ANOVA and Turkey post hoc

PC12 cells in the OGDR+MSCs group and the OGDR+MSCs+rTMS group. According to the principal component analysis (PCA) (Fig. 7A), there were significant differences among the OGDR, OGDR+MSCs, and OGDR+rTMS+MSCs groups. Besides, we also noticed that the differences between the OGDR+MSCs and OGDR+rTMS+MSCs group were also significant (Fig. 7B). As shown in the volcano diagram (Fig. 7C), We identified 240 genes that had significantly different expression genes (DEGs) in the OGDR+MSCs group compared to the OGDR+MSCs+rTMS group (fold change≥1, $p<0.05$), among which 152 genes were upregulated, and 88 genes were downregulated. Among the DEGs, Rest was one of the most significant downregulated DEGs between the OGDR+MSCs group and the OGDR+MSCs+rTMS group of PC12 neurons (Fig. 7C). We then select the most significant DEGs Egr1 and Rest and use online database genemania for protein-protein interaction (PPI) network analysis. The result showed that genes which may interact with Rest and Egr1 have a great contribution to cell proliferation [59, 60], indicating its potential role in OGDR+MSCs+rTMS treatment against neuronal death. (Fig. 7D). Genes like Mtor, Hif1a, and PIK3CA that identified promoting cell viability involved in cell viability were Rest related, according to the heat map (Fig. 7E). Further investigating the role of Rest in promoting neuron survival, we found that Rest upregulates Tubb3, which was reported to play a role in the growth of specialized nerve cell extensions called axons and dendrites [61] (Fig. 7F). And we found Rest downregulated Sp1 and Nrp1 (Fig. 7G, H). It is reported that Sp1 in astrocytes regulates the expression of many genes that are involved in neuronal developmental processes such as neurite outgrowth and synaptogenesis [62]. Nrp1 was proven to be involved in neurovascular development [63]. All of these results manifested that Rest was potentially involved in rTMS ameliorating neural death in MSCs-inhibited inflammatory conditions. Our findings shed light on the underlying mechanism of MSCs and rTMS combination treating ischemic stroke (Fig. 8).

Discussion

Cerebral ischemia is one of the leading causes of death worldwide, resulting in long-term disability among most survivors [64]. Approximately half of the survivors remain disabled ten years after ischemic stroke [65]. Additionally, up to two-thirds (or more) of patients with post-ischemic stroke suffer from neuro-dysfunction, including motor, sensory, visual, swallowing, language, cognitive, and psychological impairments [66]. rTMS has been an effective non-invasive therapy for ameliorating motor behavioral deficits for a decade [67]. MSCs, which benefit in immunological rejection, have the potential to regenerate neural function [68, 69]. Previous research reported that MSCs and TMS exerted synergistic effects in rodent models of vascular dementia, Parkinson's disease (PD), and spinal cord injury (SCI) [21, 22, 70]. The recovery of memory and learning ability of rats with vascular dementia was most significant in the application of the combined therapy compared to either therapy alone. While in the rat models of PD and SCI, combined treatment of MSCs+rTMS displayed the most executive improvement in motor function, implicating that TMS and MSCs may be more effective in neural dysfunction restoration. However, whether the combined therapy of MSCs and rTMS emerged as more effective compared with either therapy alone in ischemic stroke remains explored. Similar to previous reports, we recorded the most striking advance in motor deficit recovery in the tMCAO rat model with MSCs and rTMS combined therapy compared with those in the monotherapy group. Further pathological analysis, the TTC staining showed that the infarct size in the combined treatment group was the smallest among the three treatment groups. TTC is a photosensitive complex that acts as a proton acceptor for the pyridine-nucleoside structural enzyme system in the respiratory chain, which reacts with dehydrogenase, indicating cell viability. Thus, our data implicated that TMS and MSCs may work synergistically in protecting brain tissue from death. The following Nissl staining emphasized that the number of viable neurons was dramatically increased in the combined therapy group, suggesting a vital role in neuroprotection.

The failure of energy-dependent processes required for neuron survival is the primary cause of adverse outcomes in cerebral ischemia, especially during the acute and subacute phases [71]. Attributing to the extreme microenvironment, neurons proceed to follow either the programmed or the unprogrammed pathway of death, depending upon the degree of insult. The deprivation of ATP, oxygen, and glucose within the core ischemic region is severe and irreversible, hence, induces necrosis. While in the penumbra, this depletion hampers cellular physiological functioning but does not trigger an irreversible alternation. Neurons within the penumbra undergo apoptosis and autophagocytosis. In addition, it was observed that the activation of one pathway could simultaneously activate other pathways within the same population of neural cells [72]. Thus, characteristic death pathways along with their interaction and strategies for targeting various pathways, are crucial for promoting neural function outcomes post-ischemia. According to our data, compared to the monotherapy groups, MSCs transplantation combined with rTMS successfully inhibited several death pathways involved in the subacute phase post-ischemia, among which apoptosis, necroptosis, and pyroptosis dramatically decreased.

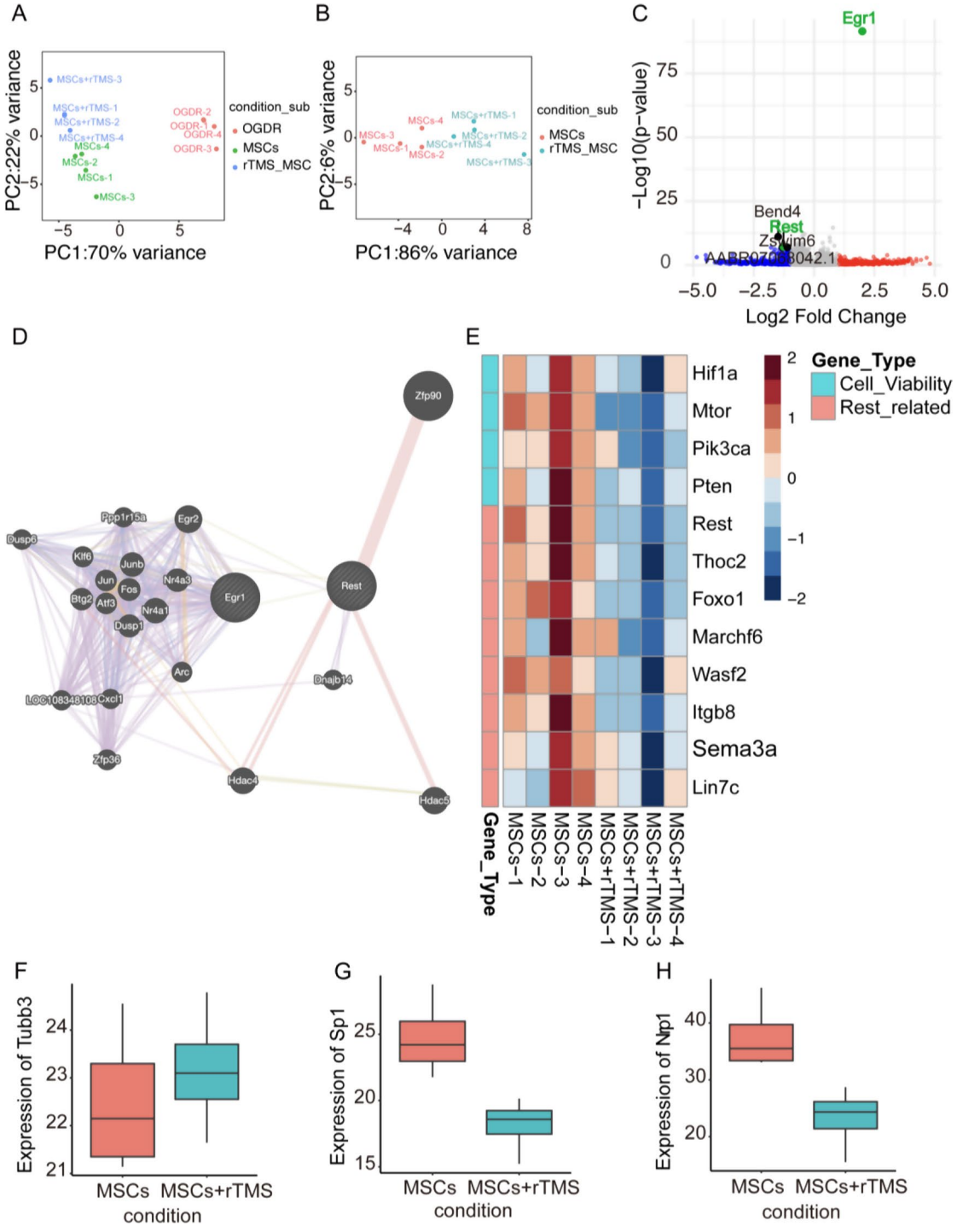

Fig. 7 rTMS ameliorates neural death in MSCs-inhibited inflammatory conditions via repressing REST. **A**, PCA analysis among the control group, the MSCs group and the MSCs + rTMS group of PC12 neurons. **B**, PCA analysis between the MSCs group and the MSCs + rTMS group of PC12 neurons. **C**, Volcano plot of DEGs between the MSCs group and the MSCs + rTMS group of PC12 neurons, the dot colored with blue means downregulated at MSCs + rTMS groups compare with MSCs while the red dots means upregulated in MSCs + rTMS groups. The grey dot means genes has no significant difference. The red dots indicate upregulated DEGs, and the blue dots indicate downregulated DEGs. **D**, PPI network analysis showed the relation of DEGs between the MSCs group and the MSCs + rTMS group of PC12 neurons. The width of each line represents the possibility of the link, the purple color means these genes were co-expressed, the red line means genes have physical interactions. The orange line was a prediction of PPI, the blue line means genes have co-localization and the light green line means these genes have shared protein domains. **E**, Heat map of DEGs involved in cell viability and Rest related between the MSCs group and the MSCs + rTMS group of PC12 neurons. **F**, **G**,**H**, Rest regulates downstream genes that involved in neuron survival

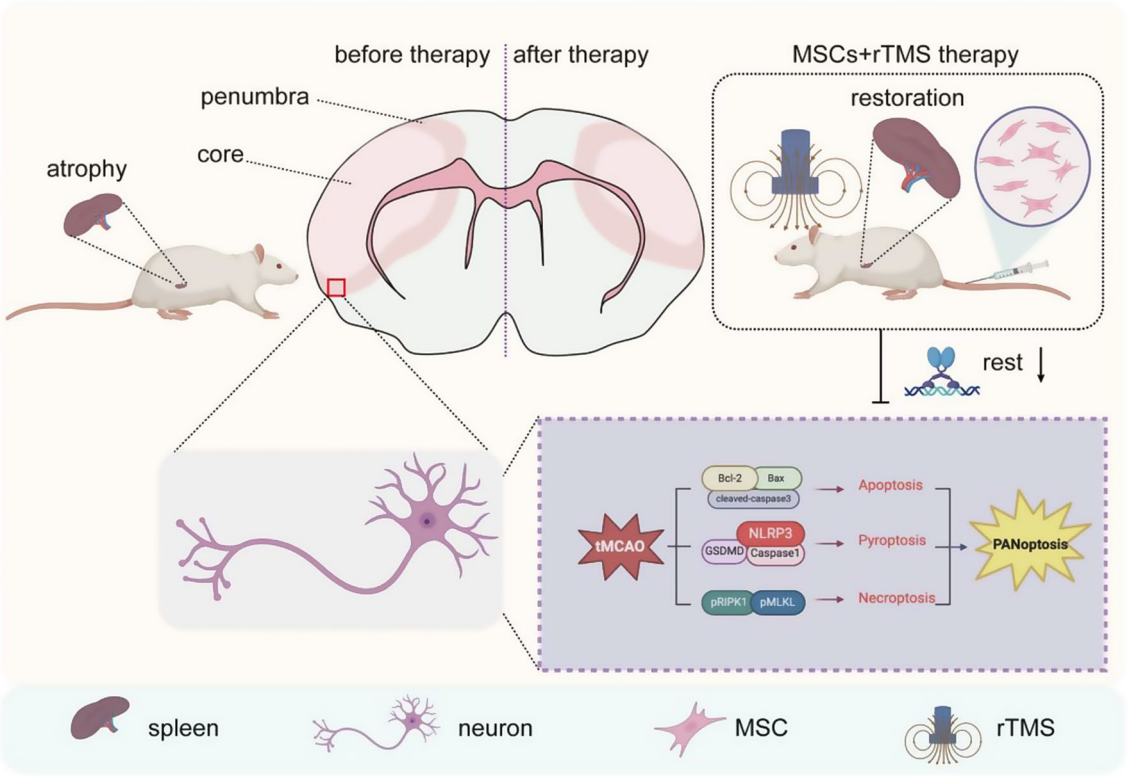

Fig. 8 Schematic diagram of the synergistic effects of MSCs and rTMS therapy against ischemic stroke

pyroptosis, apoptosis, and necroptosis consist of PANoptosis, a recently identified PCD pathway in response to various stimuli, especially neuroinflammation. Our data suggested that combined therapy is a superior therapy that may contribute to neuroprotection by inhibiting PANoptosis.

In our work, the expression level of IL-6 increased in the brain tissue but not in the serum. We hypothesized that instead of directly involving in the spleen-brain crosstalk post-ischemia, the decrease of IL-6 observed in the rTMS treatment group may be attributed to the modulation of the other IL-6 producer in the central, as reported by previous studies. For example, a study reported that rTMS reversed the down-regulation of astrocytes and inhibited high levels of IL-6, IL-1β, and TNF-α caused by chronic unpredictable mild stress (CUMS) in the above regions. Moreover, the author found that anti-inflammatory actions by rTMS were associated with the TLR4/NF-κB/NLRP3 signaling pathway [73]. Another study demonstrated that seven-days rTMS treatment reduced the level of TNF-α, iNOS, IL-1β, and IL-6 in the hippocampus of rats with CUMS [74].

The therapeutic efficacy of MSCs in neuroprotection has been demonstrated by accumulative studies [75–77]. Nevertheless, the underlying cellular and molecular mechanisms remain elusive. In the past few years, a paracrine effect of MSCs has been concluded to be a major mechanism underlying the benefits of MSC-based therapy for stroke [78]. As the paracrine of MSCs requires direct cell-cell interaction for soluble factors secretion that are involved in immune regulation, we found that few MSCs transported to the core ischemic region nor the penumbra either in the combined therapy group or MSCs monotherapy group. Instead, an accumulation of MSCs was found in the spleen, the organ responsible for cerebral inflammatory infiltration during the acute and subacute phases. Herein, we hypothesized that the decreased cerebral inflammatory infiltration observed in the combined treatment group and the MSCs monotherapy group might be attributed to the suppression of inflammation in the spleen rather than the direct interaction with neural cells. The major effect of MSCs in the combined therapy may be to prevent inflammatory infiltration from the periphery, thus protecting neurons from inflammation-induced death.

Recent studies have demonstrated that rTMS could not only provoke depolarization of the local cerebral nerve cells but also prevent glial cell activation and inhibit neuronal death [79, 80]. We observed that the effect of rTMS on preventing PC12 cell death was obviously enhanced in the MSCs co-cultured group compared to those who experienced rTMS monotherapy. Among several death pathways suppressed, apoptosis and necroptosis were

most pronounced. Thus, we suspected that rTMS is superior in neuroprotection while in an MSCs-induced low inflammation condition. The underlying mechanism of the synergistic relationship between rTMS and MSCs may be the decreased cerebral inflammatory infiltration ascribed to MSCs and the simultaneous neural death prevention attributed to the repression of repressor element-1 (RE1)-silencing transcription factor (REST) by rTMS, as revealed by RNA-Seq analysis. Cerebral ischemia is known to activate REST which silences neural genes via epigenetic remodeling and promotes neurodegeneration [81]. REST has been reported to be negatively correlated with infarct size after ischemic cerebral infarction and was an efficient target for protecting against neurons death [81, 82]. Recently, REST was identified via transcription factor network analysis as an intrinsic regulator of CNS regeneration in mice [83]. We did not find direct evidence of REST involved in PANoptosis after cerebral ischemia so far. A study demonstrated that a specific deletion of REST in podocytes exhibits podocyte apoptosis as shown by an increased expression of c-caspase3, and exhibits increased vulnerability to renal injury [84]. However, another study demonstrated that upregulating REST can eliminate the protective effect of melatonin on significantly reducing neurological deficit score and neuronal apoptosis, inhibiting CIRI autophagy, inflammation, and oxidative stress in vivo and in vitro [85]. The neurotoxicant PCB-95 by increasing the neuronal transcriptional repressor REST down-regulates caspase-8 and increases RIPK1, RIPK3, and MLKL expression determining necroptotic neuronal death [86]. Caspase-8 acts as a molecular switch for apoptosis, necroptosis, and pyroptosis. It serves as the initiator caspase for extrinsic apoptosis while inhibiting necroptosis mediated by RIPK3 and MLKL, but promoting pyroptosis and apoptosis [50]. However, we indeed observed the ASC/caspase-8/RIPK3 PANoptosome in the penumbra area during the sub-acute phase of ischemic stroke. The relationship between apoptosis, pyroptosis, and necroptosis during the sub-acute phase in ischemic stroke needs further investigation. Overall, our study demonstrated that rTMS may involve in REST downregulation and thus promoting neuron survival.

Conclusions

Our findings demonstrate that rTMS combined with MSCs transplantation could synergistically promote neuronal survival and suppress neuroinflammation in the subacute phase of cerebral infarction, thus improving neurological outcomes. rTMS may involve in REST downregulation and thus promote neuron survival.

Supplementary Information

The online version contains supplementary material available at https://doi.org/10.1186/s12974-024-03302-5.

Supplementary Material 1

Acknowledgements

This project was supported by the National Natural Science Foundation of China (Grant No. 82272605, 81972151, 82372568, and 82101367), the Natural Science Foundation of Guangdong Province (Grant No. 2023A1515030080, 2022A1515012370), and the Fundamental Research Funds for the Central Universities of Sun Yat-sen University (Grant No. 24ykqb006). We thank The Biotherapy Center for providing MSCs throughout the study. Graphical design was performed and using biorender online software (https://www.biorender.com/) with permission (agreement number: PH26WLD0TU, YU26WLCP7F; AY26WLDS7L).

Author contributions

S.C.did the main investigation, wrote the main manuscript text, and prepared Figs. 1, 2, 3, 4 and 6 and Q.Lu. wrote the main manuscript text and prepared Figs. 5 and 8 and Q.Liu. wrote the main manuscript text and provided funding; Y.M. did the biological information analysis and prepared Fig. 7;J.C. prepared part of Fig. 1; D.L. and M.H. did some investigation; Y.H., E.Z., and J.L. did some investigation; H.Z. reviewed the manuscript.All authors have reviewed the final manuscript and approved the manuscript for publication.

Data availability

The transcriptional changes in PC12 neuron cells induced by rTMS in MSCs-inhibited inflammatory conditions are publicly available in the NCBI Gene Expression Omnibus (GEO) repository (https://www.ncbi.nlm.nih.gov/geo/, accession number: GSE282396). All other data that support the findings of this study are available from the corresponding author on reasonable request.

Declarations

Ethics approval

All animal experiments were carried out according to guidelines approved by he South China Agricultural University Animal Ethics Committee (Approval no. 2022D148). No human study was performed.

Competing interests

The authors declare no competing interests.

Author details

[1]Department of Rehabilitation Medicine, The Third Affiliated Hospital, Sun Yat-Sen University, Guangzhou 510630, Guangdong, China
[2]The Biotherapy Center, The Third Affiliated Hospital, Sun Yat-sen University, Guangzhou 510630, Guangdong, China
[3]Department of Endocrinology, The First Affiliated Hospital, Sun Yat-Sen University, Guangzhou 510080, Guangdong, China
[4]Department of Gastrointestinal Surgery, The First Affiliated Hospital, Sun Yat-sen University, Guangzhou 510080, Guangdong, China

Received: 7 August 2024 / Accepted: 17 November 2024
Published online: 30 November 2024

References

1. Herpich F, Rincon F. Management of Acute Ischemic stroke [J]. Crit Care Med. 2020;48(11):1654–63. https://doi.org/10.1097/ccm.0000000000004597.
2. Candelario-Jalil E, Dijkhuizen RM, Magnus T, Neuroinflammation. Stroke, blood-brain barrier dysfunction, and imaging modalities [J]. Stroke. 2022;53(5):1473–86. https://doi.org/10.1161/strokeaha.122.036946.
3. Tsivgoulis G, Katsanos AH, Sandset EC, et al. Thrombolysis for acute ischaemic stroke: current status and future perspectives [J]. Lancet Neurol. 2023;22(5):418–29. https://doi.org/10.1016/s1474-4422(22)00519-1.

4. Wassélius J, Arnberg F, von Euler M, et al. Endovascular thrombectomy for acute ischemic stroke [J]. J Intern Med. 2022;291(3):303–16. https://doi.org/10.1111/joim.13425.
5. Eaton RG, Duru O, Powers CJ. Direct transfer for thrombectomy in patients with large vessel occlusions on computed tomography angiography results in safe revascularization [J]. Brain Circ. 2023;9(1):25–9. https://doi.org/10.4103/bc.bc_89_22.
6. Lan Z, Tan F, He J, et al. Curcumin-primed olfactory mucosa-derived mesenchymal stem cells mitigate cerebral ischemia/reperfusion injury-induced neuronal PANoptosis by modulating microglial polarization [J]. Phytomedicine. 2024;129:155635. https://doi.org/10.1016/j.phymed.2024.155635.
7. Tuo QZ, Zhang ST, Lei P. Mechanisms of neuronal cell death in ischemic stroke and their therapeutic implications [J]. Med Res Rev. 2022;42(1):259–305. https://doi.org/10.1002/med.21817.
8. Karki R, Sharma BR, Tuladhar S, et al. Synergism of TNF-α and IFN-γ triggers inflammatory cell death, tissue damage, and Mortality in SARS-CoV-2 infection and cytokine shock syndromes [J]. Cell. 2021;184(1):149–e168117. https://doi.org/10.1016/j.cell.2020.11.025.
9. Pandeya A, Kanneganti TD. Therapeutic potential of PANoptosis: innate sensors, inflammasomes, and RIPKs in PANoptosomes [J]. Trends Mol Med. 2024;30(1):74–88. https://doi.org/10.1016/j.molmed.2023.10.001.
10. Yan WT, Yang YD, Hu XM, et al. Do pyroptosis, apoptosis, and necroptosis (PANoptosis) exist in cerebral ischemia? Evidence from cell and rodent studies [J]. Neural Regen Res. 2022;17(8):1761–8. https://doi.org/10.4103/1673-5374.331539.
11. Suda S, Nito C, Yokobori S, et al. Recent advances in cell-based therapies for ischemic stroke [J]. Int J Mol Sci. 2020;21(18). https://doi.org/10.3390/ijms21186718.
12. Li Y, Huang J, Wang J, et al. Human umbilical cord-derived mesenchymal stem cell transplantation supplemented with curcumin improves the outcomes of ischemic stroke via AKT/GSK-3β/β-TrCP/Nrf2 axis [J]. J Neuroinflammation. 2023;20(1):49. https://doi.org/10.1186/s12974-023-02738-5.
13. Nakajima M, Nito C, Sowa K, et al. Mesenchymal stem cells overexpressing Interleukin-10 promote neuroprotection in experimental Acute Ischemic stroke [J]. Mol Ther Methods Clin Dev. 2017;6:102–11. https://doi.org/10.1016/j.omtm.2017.06.005.
14. Sowa K, Nito C, Nakajima M, et al. Impact of Dental Pulp Stem cells overexpressing hepatocyte growth factor after cerebral Ischemia/Reperfusion in rats [J]. Mol Ther Methods Clin Dev. 2018;10:281–90. https://doi.org/10.1016/j.omtm.2018.07.009.
15. Kuang Y, Zheng X, Zhang L, et al. Adipose-derived mesenchymal stem cells reduce autophagy in stroke mice by extracellular vesicle transfer of miR-25 [J]. J Extracell Vesicles. 2020;10(1):e12024. https://doi.org/10.1002/jev2.12024.
16. Koch G, Bonnì S, Casula EP, et al. Effect of cerebellar stimulation on Gait and Balance Recovery in patients with Hemiparetic Stroke: a randomized clinical trial [J]. JAMA Neurol. 2019;76(2):170–8. https://doi.org/10.1001/jamaneurol.2018.3639.
17. Liu Y, Luo J, Fang J, et al. Screening diagnosis of executive dysfunction after ischemic stroke and the effects of transcranial magnetic stimulation: a prospective functional near-infrared spectroscopy study [J]. CNS Neurosci Ther. 2023;29(6):1561–70. https://doi.org/10.1111/cns.14118.
18. Xie H, Li X, Xu G, et al. Effects of transcranial magnetic stimulation on dynamic functional networks in stroke patients as assessed by functional near-infrared spectroscopy: a randomized controlled clinical trial [J]. Cereb Cortex. 2023;33(24):11668–78. https://doi.org/10.1093/cercor/bhad404.
19. Zong X, Li Y, Liu C, et al. Theta-burst transcranial magnetic stimulation promotes stroke recovery by vascular protection and neovascularization [J]. Theranostics. 2020;10(26):12090–110. https://doi.org/10.7150/thno.51573.
20. Sasso V, Bisicchia E, Latini L, et al. Repetitive transcranial magnetic stimulation reduces remote apoptotic cell death and inflammation after focal brain injury [J]. J Neuroinflammation. 2016;13(1):150. https://doi.org/10.1186/s12974-016-0616-5.
21. Lee JY, Kim HS, Kim SH, et al. Combination of human mesenchymal stem cells and repetitive transcranial magnetic stimulation enhances neurological recovery of 6-Hydroxydopamine model of Parkinsonian's disease [J]. Tissue Eng Regen Med. 2020;17(1):67–80. https://doi.org/10.1007/s13770-019-00233-8.
22. Wang F, Zhang C, Hou S, et al. Synergistic effects of mesenchymal stem cell transplantation and Repetitive Transcranial Magnetic Stimulation on promoting autophagy and synaptic plasticity in vascular dementia [J]. J Gerontol Biol Sci Med Sci. 2019;74(9):1341–50. https://doi.org/10.1093/gerona/gly221.
23. Huang M, Cheng S, Li Z, et al. Preconditioning Exercise inhibits Neuron Ferroptosis and ameliorates brain ischemia damage by skeletal muscle-derived exosomes via regulating miR-484/ACSL4 Axis [J]. Antioxid Redox Signal. 2024. https://doi.org/10.1089/ars.2023.0492.
24. Huang M, Xiao C, Zhang L, et al. Bioinformatic Analysis of Exosomal MicroRNAs of Cerebrospinal Fluid in ischemic stroke rats after Physical Exercise [J]. Neurochem Res. 2021;46(6):1540–53. https://doi.org/10.1007/s11064-021-03294-1.
25. Aspey BS, Cohen S, Patel Y, et al. Middle cerebral artery occlusion in the rat: consistent protocol for a model of stroke [J]. Neuropathol Appl Neurobiol. 1998;24(6):487–97. https://doi.org/10.1046/j.1365-2990.1998.00146.x.
26. Longa EZ, Weinstein PR, Carlson S, et al. Reversible middle cerebral artery occlusion without craniectomy in rats [J]. Stroke. 1989;20(1):84–91. https://doi.org/10.1161/01.str.20.1.84.
27. Matson DJ, Broom DC, Carson SR, et al. Inflammation-induced reduction of spontaneous activity by adjuvant: a novel model to study the effect of analgesics in rats [J]. J Pharmacol Exp Ther. 2007;320(1):194–201. https://doi.org/10.1124/jpet.106.109736.
28. Waite ME, Tomkovich A, Quinn TL, et al. Efficacy of Common Analgesics for Postsurgical Pain in rats [J]. J Am Assoc Lab Anim Sci. 2015;54(4):420–5.
29. Bieber M, Gronewold J, Scharf AC, et al. Validity and reliability of neurological scores in mice exposed to Middle cerebral artery occlusion [J]. Stroke. 2019;50(10):2875–82. https://doi.org/10.1161/strokeaha.119.026652.
30. Belayev L, Alonso OF, Busto R, et al. Middle cerebral artery occlusion in the rat by intraluminal suture. Neurological and pathological evaluation of an improved model [J]. Stroke. 1996;27(9):1616–22. https://doi.org/10.1161/01.str.27.9.1616. discussion 1623.
31. Huang Y, Wang J, Cai J, et al. Targeted homing of CCR2-overexpressing mesenchymal stromal cells to ischemic brain enhances post-stroke recovery partially through PRDX4-mediated blood-brain barrier preservation [J]. Theranostics. 2018;8(21):5929–44. https://doi.org/10.7150/thno.28029.
32. Peng X, Xu H, Zhou Y, et al. Human umbilical cord mesenchymal stem cells attenuate cisplatin-induced acute and chronic renal injury [J]. Exp Biol Med (Maywood). 2013;238(8):960–70. https://doi.org/10.1177/1535370213497176.
33. Luo J, Feng Y, Hong Z, et al. High-frequency repetitive transcranial magnetic stimulation promotes neural stem cell proliferation after ischemic stroke [J]. Neural Regen Res. 2024;19(8):1772–80. https://doi.org/10.4103/1673-5374.389303.
34. Yang L, Han B, Zhang Z, et al. Extracellular vesicle-mediated delivery of circular RNA SCMH1 promotes functional recovery in Rodent and Nonhuman Primate Ischemic Stroke models [J]. Circulation. 2020;142(6):556–74. https://doi.org/10.1161/circulationaha.120.045765.
35. Luo J, Zheng H, Zhang L, et al. High-frequency repetitive transcranial magnetic stimulation (rTMS) improves functional recovery by enhancing neurogenesis and activating BDNF/TrkB signaling in ischemic rats [J]. Int J Mol Sci. 2017;18(2). https://doi.org/10.3390/ijms18020455.
36. Luo J, Feng Y, Li M, et al. Repetitive transcranial magnetic stimulation improves neurological function and promotes the anti-inflammatory polarization of Microglia in ischemic rats [J]. Front Cell Neurosci. 2022;16:878345. https://doi.org/10.3389/fncel.2022.878345.
37. Bederson JB, Pitts LH, Tsuji M, et al. Rat middle cerebral artery occlusion: evaluation of the model and development of a neurologic examination [J]. Stroke. 1986;17(3):472–6. https://doi.org/10.1161/01.str.17.3.472.
38. Bouet V, Boulouard M, Toutain J, et al. The adhesive removal test: a sensitive method to assess sensorimotor deficits in mice [J]. Nat Protoc. 2009;4(10):1560–4. https://doi.org/10.1038/nprot.2009.125.
39. Huang M, Hong Z, Xiao C, et al. Effects of exosomes on neurological function recovery for ischemic stroke in pre-clinical studies: a Meta-analysis [J]. Front Cell Neurosci. 2020;14:593130. https://doi.org/10.3389/fncel.2020.593130.
40. Barzegar M, Wang Y, Eshaq RS, et al. Human placental mesenchymal stem cells improve stroke outcomes via extracellular vesicles-mediated preservation of cerebral blood flow [J]. EBioMedicine. 2021;63:103161. https://doi.org/10.1016/j.ebiom.2020.103161.
41. Fu Y, Liu Q, Anrather J, et al. Immune interventions in stroke [J]. Nat Rev Neurol. 2015;11(9):524–35. https://doi.org/10.1038/nrneurol.2015.144.
42. Han D, Liu H, Gao Y, et al. Targeting brain-spleen crosstalk after stroke: New insights into Stroke Pathology and treatment [J]. Curr Neuropharmacol. 2021;19(9):1590–605. https://doi.org/10.2174/1570159x19666210316092225.
43. Shichita T, Ooboshi H, Yoshimura A. Neuroimmune mechanisms and therapies mediating post-ischaemic brain injury and repair [J]. Nat Rev Neurosci. 2023;24(5):299–312. https://doi.org/10.1038/s41583-023-00690-0.

44. Lee S, Karki R, Wang Y, et al. AIM2 forms a complex with pyrin and ZBP1 to drive PANoptosis and host defence [J]. Nature. 2021;597(7876):415–9. https://doi.org/10.1038/s41586-021-03875-8.
45. Sundaram B, Pandian N, Kim HJ, et al. NLRC5 senses NAD(+) depletion, forming a PANoptosome and driving PANoptosis and inflammation [J]. Cell. 2024;187(15):4061–e40774017. https://doi.org/10.1016/j.cell.2024.05.034.
46. Wei W, Wang H, Ren C, et al. Ultrasmall Enzyodynamic PANoptosis Nano-Inducers for Ultrasound-Amplified Hepatocellular Carcinoma Therapy and Lung Metastasis inhibition [J]. Adv Mater. 2024;e2409618. https://doi.org/10.1002/adma.202409618.
47. Yuan J, Ofengeim D. A guide to cell death pathways [J]. Nat Rev Mol Cell Biol. 2024;25(5):379–95. https://doi.org/10.1038/s41580-023-00689-6.
48. Shi D, Bai Y, Long R, et al. Neuronal LAMP2A-mediated reduction of adenylyl cyclases induces acute neurodegenerative responses and neuroinflammation after ischemic stroke [J]. Cell Death Differ. 2024. https://doi.org/10.1038/s41418-024-01389-0.
49. Balusu S, Horré K, Thrupp N, et al. MEG3 activates necroptosis in human neuron xenografts modeling Alzheimer's disease [J]. Science. 2023;381(6663):1176–82. https://doi.org/10.1126/science.abp9556.
50. Fritsch M, Günther SD, Schwarzer R, et al. Caspase-8 is the molecular switch for apoptosis, necroptosis and pyroptosis [J]. Nature. 2019;575(7784):683–7. https://doi.org/10.1038/s41586-019-1770-6.
51. Han Y, Yang J, Fang J, et al. The secretion profile of mesenchymal stem cells and potential applications in treating human diseases [J]. Signal Transduct Target Ther. 2022;7(1):92. https://doi.org/10.1038/s41392-022-00932-0.
52. Liang Z, Lou Y, Hao Y, et al. The relationship of astrocytes and microglia with different stages of ischemic stroke [J]. Curr Neuropharmacol. 2023;21(12):2465–80. https://doi.org/10.2174/1570159x21666230718104634.
53. Fischer MA, Davies ML, Reider IE, et al. CD11b$^+$, Ly6G$^+$ cells produce type I interferon and exhibit tissue protective properties following peripheral virus infection [J]. PLoS Pathog. 2011;7(11):e1002374. https://doi.org/10.1371/journal.ppat.1002374.
54. Wei Q, Deng Y, Yang Q, et al. The markers to delineate different phenotypes of macrophages related to metabolic disorders [J]. Front Immunol. 2023;14:1084636. https://doi.org/10.3389/fimmu.2023.1084636.
55. Simats A, Liesz A. Systemic inflammation after stroke: implications for post-stroke comorbidities [J]. EMBO Mol Med. 2022;14(9):e16269. https://doi.org/10.15252/emmm.202216269.
56. Ding Y, DeGracia D, Geng X, et al. Perspectives on effect of spleen in ischemic stroke [J]. Brain Circ. 2022;8(3):117–20. https://doi.org/10.4103/bc.bc_53_22.
57. Huang Y, Wang J, Lai X, et al. Mesenchymal stromal cells attenuate post-stroke infection by preventing caspase-1-dependent splenic marginal zone B cell death [J]. Signal Transduct Target Ther. 2021;6(1):60. https://doi.org/10.1038/s41392-020-00415-0.
58. Donovan JA, Koretzky GA. CD45 and the immune response [J]. J Am Soc Nephrol. 1993;4(4):976–85. https://doi.org/10.1681/asn.V44976.
59. Milde T, Oehme I, Korshunov A, et al. HDAC5 and HDAC9 in medulloblastoma: novel markers for risk stratification and role in tumor cell growth [J]. Clin Cancer Res. 2010;16(12):3240–52. https://doi.org/10.1158/1078-0432.Ccr-10-0395.
60. Piechaczyk M, Farràs R. Regulation and function of JunB in cell proliferation [J]. Biochem Soc Trans. 2008;36(Pt 5):864–7. https://doi.org/10.1042/bst0360864.
61. Radwitz J, Hausrat TJ, Heisler FF, et al. Tubb3 expression levels are sensitive to neuronal activity changes and determine microtubule growth and kinesin-mediated transport [J]. Cell Mol Life Sci. 2022;79(11):575. https://doi.org/10.1007/s00018-022-04607-5.
62. Hung CY, Hsu TI, Chuang JY, et al. Sp1 in astrocyte is important for Neurite Outgrowth and synaptogenesis [J]. Mol Neurobiol. 2020;57(1):261–77. https://doi.org/10.1007/s12035-019-01694-7.
63. Raimondi C, Brash JT, Fantin A, et al. NRP1 function and targeting in neurovascular development and eye disease [J]. Prog Retin Eye Res. 2016;52:64–83. https://doi.org/10.1016/j.preteyeres.2016.02.003.
64. Feigin VL, Owolabi MO. Pragmatic solutions to reduce the global burden of stroke: a World Stroke Organization-Lancet Neurology Commission [J]. Lancet Neurol. 2023;22(12):1160–206. https://doi.org/10.1016/s1474-4422(23)00277-6.
65. Hardie K, Hankey GJ, Jamrozik K, et al. Ten-year risk of first recurrent stroke and disability after first-ever stroke in the Perth Community Stroke Study [J]. Stroke. 2004;35(3):731–5. https://doi.org/10.1161/01.Str.0000116183.50167.D9.
66. Global regional. Lancet Neurol. 2021;20(10):795–820. https://doi.org/10.1016/s1474-4422(21)00252-0. and national burden of stroke and its risk factors, 1990–2019: a systematic analysis for the Global Burden of Disease Study 2019 [J].
67. Sheng R, Chen C, Chen H, et al. Repetitive transcranial magnetic stimulation for stroke rehabilitation: insights into the molecular and cellular mechanisms of neuroinflammation [J]. Front Immunol. 2023;14:1197422. https://doi.org/10.3389/fimmu.2023.1197422.
68. Jaillard A, Hommel M, Moisan A, et al. Autologous mesenchymal stem cells improve Motor Recovery in Subacute Ischemic Stroke: a Randomized Clinical trial [J]. Transl Stroke Res. 2020;11(5):910–23. https://doi.org/10.1007/s12975-020-00787-z.
69. Walczak P, Zhang J, Gilad AA, et al. Dual-modality monitoring of targeted intraarterial delivery of mesenchymal stem cells after transient ischemia [J]. Stroke. 2008;39(5):1569–74. https://doi.org/10.1161/strokeaha.107.502047.
70. Feng S, Wang S, Sun S, et al. Effects of combination treatment with transcranial magnetic stimulation and bone marrow mesenchymal stem cell transplantation or raf inhibition on spinal cord injury in rats [J]. Mol Med Rep. 2021;23(4). https://doi.org/10.3892/mmr.2021.11934.
71. Eren F, Yilmaz SE. Neuroprotective approach in acute ischemic stroke: a systematic review of clinical and experimental studies [J]. Brain Circ. 2022;8(4):172–9. https://doi.org/10.4103/bc.bc_52_22.
72. Al-Abdulla MLJ, Brambrink NA. Neurodegeneration in excitotoxicity, global cerebral ischemia, and target deprivation: a perspective on the contributions of apoptosis and necrosis [J]. Brain Res Bull. 1998;46(4):281–309. https://doi.org/10.1016/s0361-9230(98)00024-0.
73. Zuo C, Cao H, Feng F, et al. Repetitive transcranial magnetic stimulation exerts anti-inflammatory effects via modulating glial activation in mice with chronic unpredictable mild stress-induced depression [J]. Int Immunopharmacol. 2022;109:108788. https://doi.org/10.1016/j.intimp.2022.108788.
74. Tian L, Sun SS, Cui LB, et al. Repetitive transcranial magnetic stimulation elicits antidepressant- and anxiolytic-like Effect via Nuclear Factor-E2-related factor 2-mediated anti-inflammation mechanism in rats [J]. Neuroscience. 2020;429:119–33. https://doi.org/10.1016/j.neuroscience.2019.12.025.
75. Son JW, Park J, Kim YE, et al. Glia-like cells from late-passage human MSCs protect against ischemic stroke through IGFBP-4 [J]. Mol Neurobiol. 2019;56(11):7617–30. https://doi.org/10.1007/s12035-019-1629-8.
76. Shen LH, Li Y, Chen J, et al. One-year follow-up after bone marrow stromal cell treatment in middle-aged female rats with stroke [J]. Stroke. 2007;38(7):2150–6. https://doi.org/10.1161/strokeaha.106.481218.
77. Otero-Ortega L, Gutiérrez-Fernández M, Ramos-Cejudo J, et al. White matter injury restoration after stem cell administration in subcortical ischemic stroke [J]. Stem Cell Res Ther. 2015;6(1):121. https://doi.org/10.1186/s13287-015-0111-4.
78. Liang X, Ding Y, Zhang Y, et al. Paracrine mechanisms of mesenchymal stem cell-based therapy: current status and perspectives [J]. Cell Transpl. 2014;23(9):1045–59. https://doi.org/10.3727/096368913x667709.
79. Luo L, Liu M, Fan Y, et al. Intermittent theta-burst stimulation improves motor function by inhibiting neuronal pyroptosis and regulating microglial polarization via TLR4/NFκB/NLRP3 signaling pathway in cerebral ischemic mice [J]. J Neuroinflammation. 2022;19(1):141. https://doi.org/10.1186/s12974-022-02501-2.
80. Buetefisch CM, Wei L, Gu X, et al. Neuroprotection of Low-Frequency Repetitive Transcranial Magnetic Stimulation after ischemic stroke in rats [J]. Ann Neurol. 2023;93(2):336–47. https://doi.org/10.1002/ana.26509.
81. Morris-Blanco KC, Kim T, Bertogliat MJ, et al. Inhibition of the Epigenetic Regulator REST ameliorates ischemic Brain Injury [J]. Mol Neurobiol. 2019;56(4):2542–50. https://doi.org/10.1007/s12035-018-1254-y.
82. Noh KM, Hwang JY, Follenzi A, et al. Repressor element-1 silencing transcription factor (REST)-dependent epigenetic remodeling is critical to ischemia-induced neuronal death [J]. Proc Natl Acad Sci U S A. 2012;109(16):E962–971. https://doi.org/10.1073/pnas.1121568109.
83. Cheng Y, Yin Y, Zhang A, et al. Transcription factor network analysis identifies REST/NRSF as an intrinsic regulator of CNS regeneration in mice [J]. Nat Commun. 2022;13(1):4418. https://doi.org/10.1038/s41467-022-31960-7.
84. Magassa S, Aron L, Hoguin C, et al. REST and Stress Resistance in the aging kidney [J]. J Am Soc Nephrol. 2021;32(8):1974–86. https://doi.org/10.1681/asn.2021020231.
85. Yang B, Zang LE, Cui JW, et al. Melatonin plays a protective role by regulating miR-26a-5p-NRSF and JAK2-STAT3 pathway to improve autophagy, inflammation and oxidative stress of Cerebral Ischemia-Reperfusion Injury [J]. Drug Des Devel Ther. 2020;14:3177–88. https://doi.org/10.2147/dddt.S262121.

86. Guida N, Laudati G, Serani A, et al. The neurotoxicant PCB-95 by increasing the neuronal transcriptional repressor REST down-regulates caspase-8 and increases Ripk1, Ripk3 and MLKL expression determining necroptotic neuronal death [J]. Biochem Pharmacol. 2017;142:229–41. https://doi.org/10.1016/j.bcp.2017.06.135.

Publisher's note